Numerical Modeling of the Long-term Transport, Dispersion and Accumulation of Black Sea Pollutants into the North Aegean Coastal Waters

Kyriakos I. Kopasakis[1], Anastasios N. Georgoulas[1], Panagiotis B. Angelidis[1], Nikolaos E. Kotsovinos[1],

[1] *Laboratory of Hydraulics and Hydraulic Structures,*
Democritus University of Thrace, Department of Civil Engineering, V. Sofias 12
GR-67 100 Xanthi, Greece

Abstract

This study investigates the long-term capacity of the North Aegean coastal systems to transport and store conservative pollutants that originate from the Black Sea. Emphasis is placed on modeling the dispersion and accumulation of a passive tracer that represents a Black Sea Pollutant (BSP) substance that continuously discharges from the Dardanelles exit into the North Aegean, for a long period of time (16 years). The effects of the Black Sea Water (BSW) inflows, meteorological forcing and seasonal stratification are assessed with a 3D hydrodynamic model (ELCOM), after validation with available field data. The salinity, the water temperature and discharge from the Dardanelles straits are taken to be seasonally varied. According to the authors best knowledge the present paper constitutes the first numerical modeling attempt in the literature that apart from the long-term hydrodynamic characteristics that have also been studied in previous works, a suitable tracer is introduced in order to predict the long term fate, distribution and accumulation of pollutants that originate from the Black Sea, into the North Aegean coastal regions. The overall results of the present investigation indicate that the BSP concentration is very high at the coastal waters of Thassos, Samothraki and Limnos islands, as well as along the mainland coastal waters between Alexandroupolis and Strymonikos Gulf, during summer and autumn when strong water column stratification occurs. In general, the Black Sea Pollutant (BSP) concentration in the North Aegean surface waters reaches considerable high values (47%-58% of the initial pollutant concentration at Dardanelles inflow) within 16 years. Even for depths more than 500m the BSP concentration is still remarkable, slightly increasing with time. The increase of the BSP concentration with respect to time at various depths (from free surface up to 750 m) is also investigated.

Keywords: North Aegean, Black Sea Pollutant, Dardanelles, conservative tracer, transport, surface buoyant plume.

1. Introduction

As with much of the Eastern Mediterranean Sea, the Aegean Sea is considered to be an oligotrophic basin. The flow of colder and less saline water from the Black Sea through the Turkish straits (Bosporus and Dardanelles Straits) and the Sea of Marmara, tends to cool mostly the surface water and reduce the high surface salinity of the North Aegean Sea. This brackish surface water discharge, from the Black Sea through the Dardanelles Straits into the North Aegean Sea, constitutes one of the major factors that affect the North Aegean water column (Ignatiades et al., 2002; Ignatiades, 2005).

The ecological situation of the Black Sea region depends on geographical reasons as well as on the influence of various anthropogenic activities. Over the past decades the Black Sea has increasingly attracted the attention of scientists, governments and the public at large, as a region that suffers from ecological deterioration (Zaitsev and Mamaev, 1997). The Black Sea basin is suffering by excessive loads of nutrients flowing from rivers such as the Danube, Dniper, Dnister, etc. (Ludwig et al., 2009). In addition, around 111,000 tons of oil enters the Black Sea each year, while the amount of oil reaching the Black Sea from ballast water discharges by ships is unknown but it is believed to be considerable. The present ecological situation of the Black Sea in relation to increased shipping from ports in the Black Sea and the prospect of considerably higher tanker traffic carrying Caspian and Central Asian oil through the Aegean, have generated fears in Greece and Turkey, as well as among environmentalists throughout the world, of still more acute threats to the ecosystem and cleanliness of the Aegean (Zaitsev and Mamaev, 1997).

There are two types of potential pollution in the North Aegean Sea as a result of the dense sea traffic in the Turkish Straits and the ecological situation in the Black Sea. The first is connected with the increasing accidents in the Turkish Straits and the unavoidable pollution they cause (Alper et al., 2006). The second concerns the brackish waters and pollutant discharge, from the Black Sea, that enter in to the North Aegean Sea via the Dardanelles Straits (Birpinar et al., 2006). Therefore, there is a strong need for the development of monitoring, simulation and evaluation tools, to assess the long term effectiveness of the BSW discharge for carrying, transporting, dispersing and accumulating pollutants in the coastal areas of the North Aegean. One of the key steps in this unresolved research aspect is the determination of the long-term carrying capacity of the North Aegean coastal systems, to transport and store the Black Sea conservative pollutants.

Hydrodynamic modeling of large scale outflows that transport pollutants in the

complex estuarine and ocean environment has become more realistic as computational speed has increased. Up to present, there are various numerical investigations dealing with the hydrodynamic circulation in the North Aegean Sea. A first approach towards an ocean forecasting system for the Aegean Sea has been presented by Korres et al. (2002). The proposed ocean forecasting component is part of the POSEIDON system, which includes high resolution atmospheric and wave modeling of the Aegean Sea together with an extended network of observational buoys, for the continuous monitoring of physical, biological and chemical parameters. The POSEIDON system is a modern oceanographic system that has established a network of observation buoys as well as a specialized Greek operational center for the processing of the data collected and the production of forecasts. The network of observation buoys records continuously the physical, biological and chemical parameters of the Greek seas. Those data are then transmitted to the operational center where they are sorted and fed into suitable forecasting models. In more detail, the ocean forecast model system consists of a high-resolution (1/20° × 1/20° that corresponds to 4.1-4.8 km by 5.3-5.7 km horizontal computational grid) implementation of the Princeton Ocean Model (POM), forced by forecast surface fluxes of momentum, heat and freshwater provided by the regional ETA atmospheric model.

The seasonal characteristics of the circulation in the North Aegean Sea are examined with the aid of a climatological type simulation on a fine resolution grid (2.5 km by 2.5 km) in the work of Kourafalou and Barbopoulos (2003).

In the work of Kanarska and Maderich (2008) the POM model is applied to study the seasonal hydrodynamics variability in the Dardanelles straits. It is found that the seasonal exchange dynamics is governed by the turbulent friction and entrainment at the narrowest part of the Dardanelles Straits.

Furthermore, in the work of Androulidakis et al. (2011) the numerical model NAS-HYCOM (Hybrid Coordinate Ocean Model), is implemented to perform process-oriented experiments that examine the relative role of the forcing factors and topographic effects along the North Aegean shelf areas.

Blain et al. (2009) have coupled the Advanced Circulation Model (ACIRM) and HYCOM to model the Black Sea plume that outflows from the Dardanelles Straits into the North Aegean Sea. Finally, the impact of the BSW inflow on the circulation and the water mass characteristics of the North Aegean Sea, is investigated using POM in the work of Tzali et al. (2010). A horizontal computational grid of 1/60°x1/60° is used to perform four climatological numerical experiments, exploring the effects of the exchange amplitude at the

Dardanelles Straits in terms of the mean annual volume exchanged and the amplitude of its seasonal cycle.

Considerable advances have been made during the last decades for the development of the required tools for the prediction of the hydrodynamics in the North Aegean coastal water, namely three-dimensional hydrodynamic models. However, there is a large gap in the literature concerning the transport and dispersion of pollutants that originate from the Black Sea and end up in the coastal waters of the mainland and the islands of the North Aegean. The aim of the present study is to investigate the dispersion rate of the brackish, surface-evolving Black Sea plume in the North Aegean water column, using the 3D hydrodynamic model ELCOM, focusing in the evaluation of the long-term distribution of conservative pollutants that originate from the Back Sea, in the coastal waters of the North Aegean, that according to the authors best knowledge has not been assessed previously. It should also be mentioned that the Coriolis force effect is taken into consideration.

The choice of the 3D hydrodynamic model ELCOM was made due to its advanced ability to monitor and predict the Black Sea pollutants that outflow in the North Aegean Sea using passive non-dimensional computational Tracers. This technique, according to the authors' best knowledge, is the first approach of evaluating the fate of the Black Sea pollutants that reach and disperse to the North Aegean Coastal Areas.

2. Model description

2.1. Description of the hydrodynamic model ELCOM

The ELCOM (Estuary, Lake and Coastal Ocean Model) that is used for the numerical simulation of the present paper, is a three-dimensional hydrodynamic model for estuaries, lakes and enclosed seas and is used to predict the variation of water temperature, salinity or transport of tracers/drifters in space and time (Hodges and Dallimore 2010b). It applies hydrodynamic and thermodynamic models for the simulation of the temporal behavior of stratified water bodies with environmental forcing. The hydrodynamic simulation method solves the unsteady, viscous Navier-Stokes equations for incompressible flows using the hydrostatic assumption for pressure. Modeled and simulated processes include baroclinic and barotropic responses, rotational effects, tidal forcing, wind stresses, surface thermal forcing, inflows, outflows, and transport of salt, heat and passive scalars. The hydrodynamic algorithms are based in a semi-implicit, finite-difference approach and on a second-order

Euler-Lagrange advection of momentum, with an implicit solution of the free surface evolution. Passive and active scalars (i.e. tracers, salinity and temperature) are advected using the conservative ULTIMATE QUICKEST discretization. The transport equations are the unsteady Reynolds-averaged Navier-Stokes (RANS) as well as scalar transport equations, using the Boussinesq approximation and neglecting the non-hydrostatic pressure terms. The free surface evolution is governed by a vertical integration of the continuity equation applied to the Reynolds-averaged kinematic boundary condition.

Heat exchange at the atmosphere-ocean interface is separated into penetrative (solar radiation) and non penetrative components (long wave radiation and sensible and latent heat fluxes). Solar radiation penetrates into the water, following an exponential decay as described by Beer's Law (Imberger and Patterson, 1990). Sensible and evaporative heat losses are variable across the water surface and are described by standard bulk transfer equations that are corrected to account for the effects of atmospheric stability (Imberger and Patterson, 1990). The user is required to supply meteorological information (e.g. solar radiation, wind-speed and direction, humidity and air temperature) and inflow and outflow volume fluxes.

The computation of the model time step is made in a staged approach and surface heating and cooling in the surface layer are introduced. The computational grid may consist of rectangular cells with both uniform and non-uniform grid spacing in the vertical and horizontal direction. The solution is based in the Arakawa C-grid stencil, where velocities are defined on cell faces with the free surface height and scalar values on cell centers. The free surface height in each column of grid cells moves vertically at the surface grid layer, as required by the free-surface evolution equation (Hodges and Dallimore, 2010a).

ELCOM is implemented in Fortran 90 so that three-dimensional space can be mapped into a single vector for fast operation, using array-processing techniques. Only the computational cells that contain water are represented in the single vector so that memory usage can be minimized. This allows Fortran 90 compiler parallelization and vectorization, without platform-specific modification of the code (Imberger and Patterson, 1990).

2.2. Description of model inputs and set up

The selected region of the North Aegean Sea that is used for the numerical simulation of the present investigation is depicted in Figure 1. As it can be seen it is bounded to the north and west by the Greek mainland and to the east by the Turkish coastline. The south open sea boundary is located before the south end of Chios Island. A rectangular computational grid

was constructed, consisting of uniformly distributed horizontal cells with a breadth and width of 4 km, (Figure 1). In the vertical direction 200 layers of 5m thickness each, were used. Therefore, the first 1000m depth are taken into account for the simulation. According to Hodges and Dallimore (2010a), such a fine homogeneous grid in the vertical direction performs better and gives more accurate results than a non-homogeneous grid. The choice of such a fine vertical grid was made in order to study with great accuracy, the evolution of the water column stratification and the tracer's long-term vertical concentration distribution in the lower sea water layers. On the other hand, a grid dependency analysis, comparing finer and coarser as well as homogeneous and non-homogeneous grids in the horizontal and vertical direction) indicated minor differences in the results with the adopted grid. Moreover the adopted, uniformly distributed grid indicated a large gain in computational efficiency and stability during the calculations, in relation to the non-uniform cases tested. In the bottom layer a turbulent benthic boundary condition was applied, while the viscosity value was taken to be constant. To avoid numerical diffusion during the calculations the constructed numerical grid is rotated 17.48 degrees clockwise from the north, in order for the Dardanelles outflow to be parallel to the horizontal grid lines.

The selected time step for the calculations is 3min and a total real flow time of 16 years is simulated. The starting date for the simulation is selected to be the beginning of winter on 1 January 2005, when the water column was well-mixed and freshwater inputs were confined to the eastern margins. The corresponding ending date is selected to be on 31 December 2020. Winter is defined as December to February, spring as March to May, summer as June to August and autumn as September to November. The BSW entering the model domain via the Dardanelles Straits and the water of the North Aegean Sea exiting the model domain at the Hellespont, are simulated as point sources. The river inflows in the North Aegean Sea are neglected, as they can be considered negligible in relation to the massive mean annual discharge from the Dardanelles Straits. Daily discharges, available in the literature (Kanarska and Maderich, 2008), are used for inflows and outflows at the Dardanelles exit to the North Aegean.

The maximum and minimum discharges in the upper layer occur in winter and summer, respectively. Mean annual values of the discharges at the Aegean exit are at about 38820 m^3/s in the upper layer (from the Dardanelles into the Aegean) and 30000 m^3/s in the bottom layer (from the Aegean into the Dardanelles). The seasonal variability of volume fluxes in the bottom layer of the Aegean exit is 9600 m^3/s. The variability of the discharges in the upper layer is much weaker (about 6115 m^3/s). These differences could be explained by

the contribution of the baroclinic component that causes density differences between the two basins (Unluata et al., 1990; Kanarska and Maderich, 2008). The water inflow (from the Dardanelles into the Aegean) takes place within the first 10m depth, while the water outflow (from the Aegean into the Dardanelles) takes place from 10m to 55m depth.

The movement and dilution of the Dardanelles inflow is tracked using a conservative tracer. In general, a conservative tracer has no decay and therefore its contribution is controlled solely by currents, wind energy, and mixing. This conservative, passive tracer, which is called Tracer 1, represents the pollutant inflow from the Dardanelles from the beginning of the simulation, in the form of a dimensionless concentration varying from 0 (at the Aegean) to 1 (at the Dardanelles exit).

2.3. Initial conditions, boundary conditions and forcing fields

Initial conditions over the whole model domain were taken from varying temperature and homogeneous salinity values that were derived from literature sources (Kanarska and Maderich, 2008). Since the simulation begins on January of 2005 the initial condition for the water temperature and salinity according to the work of Kanarska and Maderich (2008) were assumed to be 12.5°C and 38.9 psu respectively.

The open boundary condition for the model domain was selected at the boundary between the Northern and Southern basins (Figure 1), to minimize boundary-forcing effects on the main area of interest, in the Dardanelles outflow as well as in the circulation patterns of the North Aegean Sea. Model inputs for this boundary included homogeneous profiles of temperature and salinity derived from field measurements at stations in the islands of Skyros and Mitilini by the Poseidon system of the Hellenic Centre of Marine Research. Typical salinity and temperature profile values used as open southern boundary forcing conditions, for 3 years of simulation (2008-2010), are depicted in Figures 2a, 2b. It should be mentioned that for simplicity purposes, the values that were actually applied for the southern open boundary condition forcing are those referred to the average value graph (Black curve at Figures 2a and 2b).

The two-layer exchange flow at Dardanelles is primarily controlled by mixing and friction at a much shorter time scale. In other words, the magnitude of Dardanelles outflow alters daily in response to local environmental conditions, such as the short term wind episodes. Therefore, in order to treat more realistically the impact of the Dardanelles outflow

in the North Aegean, a high frequency (daily) superimposed forcing was applied for the outflow and inflow boundary conditions.

A 6 year period (2005-2010) of meteorological data consisting of 10 minutes frequency readings of wind speed, wind direction, solar radiation, air pressure, air temperature, relative humidity and rainfall height, measured at the Genisea meteorological station at North Greece, were applied over the whole domain for the corresponding simulation period (2005-2010). Genisea station is stated in the city of Xanthi and belongs to the Hydraulics Division of the Department of Civil Engineering in the Democritus University of Thrace (Greece). An example of these meteorological data are given in Figure 3 and Figure 4 indicatively for the year 2010. It should be mentioned that for the decade 2011-2020, the meteorological data are assumed to be the same with those recorded from the Genisea station for the period 2001-2010.

3. Model validation

The model validation and calibration was made by comparing the modeled hydrodynamic results with field data derived from literature sources. Quantitative assessment of the model performance in reproducing field measurements, was performed by evaluating the r^2 (determination coefficient). The vertical distribution of water salinity and temperature was validated on local as well as on regional scales. Finally, modeled surface water circulation was validated with Sea Surface Circulation (SC) images, generated from the Poseidon system of the Hellenic Centre for Marine Research.

The development of summer stratification, winter overturn and intermediate transitional periods is evident in measured and simulated water temperature and salinity time series (Figure 5) at Poseidon Athos Station Northwest of Limnos Island, for various water depths. As it can be seen, the predicted by the model time periods that the creation and breakdown of stratification take place was May and January respectively, in agreement with the corresponding observations at the Athos station. Coefficients of determination r^2 for salinity and temperature profiles over the year 2009 were 0.65-0.74 and 0.75-0.99 respectively, indicating that the model adequately reproduces the observed values (Figures 6a, 6b).

Figure 7 illustrates the comparison between modeled average water temperature and salinity and measured average water temperature and salinity for a range of depths at 3 stations (L.1, L.2, L.3) stated at east of Limnos Island on December of 2005. The measured

data were derived from Evangeliou et al., (2009) field investigations. Comparisons of the model results with field data from the field work of Evangeliou et al., (2009) were also made for June 2006, regarding the density profiles at stations L.1, L.2, L.3 as it is shown in Figures 8a, 8b and 8c. The position of the corresponding sampling stations can be found in the work of Evangeliou et al. (2009). The modeled data of Figure 7 and Figure 8 correspond to the same time period that the seawater samples were collected during the cruises. According to Figures 7a, 7b, 7c the average water temperature, at stations L.1, L.2 and L.3, varied between 14.2°C to 16.2°C for a depth range between 4m to 65m. The small variation of the water temperature shows once again that a full-mixed water column occurs during winter. The relatively lower average surface salinity and temperature values at station L.1 in Figures 7a, 7d constitute a characteristic evidence of the BSW effect in the specific area. The simulated temperature and salinity profiles at the stations L.1, L.2 and L.3 compare well with the corresponding measured profiles (r^2= 0.70-0.98 and r^2= 0.65-0.74) according to Figures 9a and 9b.

Density profiles had the best fit in the quantitative comparison of the model predictions with the measured data (Figure 9c). The model was able to predict 96%-98% of the measured density variability in the calibration month of June 2006 (r^2=0.96-0.99). The steep density gradients at the first 20m depth at stations L.1, L.2, L.3 (Figures 8a, 8b, 8c), prove the presence of the Black Sea plume in the region and the high water column stratification that is developed during the summer period.

Modeled velocities of the surface currents were validated with the CORI (Prevention and Management of Sea Originated Risks to the Coastal Zone) surface current measuring system of Poseidon, on the east coast of Limnos Island according to Figure 10 (Hellenic Centre for Marine Research, 2010). Comparisons of the corresponding images show that the model successfully captures the main flow schemes that are derived from CORI, both in velocity magnitude and direction. In more detail during February the inflow from the Dardanelles Straits splits in two streams (Figures 10a, 10c). The first stream is directed south to Limnos Island and the second stream passes through the islands of Limnos and Gokceada (Imvros), and then experiences either a clockwise eddy or continue in a northward jet-like pattern. The anticyclonic eddy that happens in the region between the islands of Limnos and Imvros during September is depicted in Figures 10b, 10d.

4. Results and discussion

A long period of real flow has been simulated in order to investigate a possible scenario of pollution due to the BSP inflow and gain knowledge regarding the influence of the North Aegean Sea region hydrodynamics on the fate of the proposed pollution input. The scenario studied corresponds to a continuous pollution by the direct Black Sea seasonal pollutant discharge into the North Aegean, through the Dardanelles Straits.

4.1. Numerical modeling results for the North Aegean Coastal Zone

4.1.1. Hydrodynamic characteristics of the North Aegean Coastal Zone

As previously stated, the dynamics of the North Aegean Coastal Zone is determined to a large extend by the flow of the surface buoyant plume that is formed by the brackish Black Sea water discharge into the North Aegean Sea, through the Dardanelles Straights. The salinity distribution evolves with the water circulation and the fluctuations of the wind field. Southerly winds together with the Coriolis force effect, force the larger part of the proposed plume along the North Aegean coastline, while northerly winds have a blocking effect and push the plume further offshore.

According to Figures 11 and 12 and in agreement with previous investigations by Koukouras et al. (1984) and Sylaios et al. (2006), the North Aegean Coastal Zone and especially the area surrounding Alexandroupolis, Maronia, Kavala Gulf, Strimonikos Gulf and Athos peninsula shows significant temporal variability patterns in physical parameters, as a result of the less saline surface water that originates from the Black Sea. In these figures the horizontal axis concerns the distance in km along the coastline in a counter-clockwise direction and with the zero value located at the Dardanelles exit. More specific, in Figure 11, a branch of this low salinity surface is depicted, varying from 35.9 psu at Alexandroupolis during June to 37.9 psu at Athos peninsula during April.

The salinity at the surface of the Thracian coastal area (Figure 11) shows slightly higher values in comparison with the salinity values at the rest of the North Aegean surface area on January and April, while on October the salinity is reduced since it is generally influenced by the seasonal variations of the salinity at the Dardanelles Straits exit (Kanarska and Maderich, 2008). Especially during summer the surface layer is warmer than the water masses that occupy deeper depths. This temperature variation in the water column of the

North Aegean is the main reason of the strong stratification that is developed during the summer period. The development of the water column stratification leads to the BSW isolation in the upper layers and subsequently its accumulation in shallow water depths in the North Aegean coastal area.

In Thermaikos Gulf the surface salinity is influenced by the BSW plume in a comparatively lower grade, with values varying in a relatively small range between 38.15 psu in April to 38.65 psu in October. This observation indicates that the seasonality of the BSW plume has small effect in the surface salinity and water density in the Thermaikos Gulf. In general, as far as the distance of the North Aegean Coastal Zone from the release point of the Black Sea outflow (Dardanelles Straits) increases, the salinity increases indicating that the BSW plume is less effective.

The main feature of the circulation in the North Aegean Sea is the BSW current, with surface velocities up to 0.4 m/sec. ELCOM maps of density and current velocity in the surface water layer (Figure 13) indicate the development of the lower density tongue of BSW, during the late spring and summer period, arrested by the permanent gyres that flow along the North Aegean Coastal Zone. These are, the anticyclonic movement of the BSW west of Limnos Island (Figure 13c), the small scale anticyclonic gyre of the BSW between Limnos Island and Gokceada (Imvros) Island (Figure 13c), the cyclonic gyre within the Thermaikos Gulf (Figure 13d), the anticyclone that is formed around the Samothraki Island (the Samothraki gyre) (Figure 13e) and the cyclonic gyre that is acting east of Thasos Island (Figure 14).

The snapshot of the simulated salinity and current velocity distribution shown in Figure 15 represents the instantaneous pattern of the BSW plume on 16th of September of 2010. As it can be derived also from field observations (Olson et al., 2006; Isari et al., 2006 and Sylaios et al., 2006), the brackish BSW plume is swept along in an anticlockwise residual gyre, off the Thracian coastline. When leaving the Dardanelles Straits, a part of the plume turns to the right and flows along the Thracian coast towards the Strimonikos Gulf. Another branch of the plume is directed east to Limnos Island, then turns right and with the influence of the Samothraki strong anticyclonic gyre enhances the BSW plume at the Thracian coastal waters. In Thermaikos Gulf the presence of the BSW plume is influenced by the North Sporades eddy rotation (Figure 15). Thus, according to the model results, September is the only month that shows evidence of a relatively strong salinity front, due to the intrusion of BSW that extends to the Sporades basin and is associated with the north Sporades cyclone in

agreement with Kontoyiannis et al. (2003). This finding also agrees with the findings by Kourafalou and Barbopoulos (2003) and more recently by Olson et al. (2006).

4.1.2. Conservative tracer distribution in the Coastal Zone of the North Aegean

As mentioned previously, in the present study a long term simulation have been carried out to investigate possible scenarios of pollution in the North Aegean Coastal Area and learn more about the influence of the hydrodynamics on the fate of this pollution. Thus, the model ran for a total real flow period of 16 years, starting on 01 January 2005.

As an example a constant release of conservative Tracer were considered at the Dardanelles exit. During the entire period of tracer's release, their dimensionless concentration was set to unity (maximum value) at the inflow area (0-10m depth). The flow rate of the BSW plume, at this point, is seasonally varied according to the inflow discharge. The studied scenario corresponds to the case of a continuous pollution by the direct discharge of pollutants in the Dardanelles Straits from the Black Sea through the Bosporous Straits and the Sea of Marmara or by a possible accident in the area of Dardanelles Straits, which pollutes in a constant rate for a long period of time. The passive tracer (Tracer 1), which from now on will be called BSP (Black Sea Pollutant), is then transported to the North Aegean Sea through the BSW plume with a large amount being accumulated in the North Aegean coastal waters.

The distribution of the conservative BSP concentration in the coastal waters of the North Aegean depends on the Coriolis force which forces the BSW plume to move northwards to the Thracian coastal waters, the flow characteristics of the BSW plume and the wind speed and direction which influence the BSP diffusion rate.

Figure 16, presents the vertical distribution of the average BSP dimensionless concentration with respect to time for the entire simulation period and for the whole North Aegean domain. The BSP concentration appears to be very high, around 37-58% of its inflow value within the upper water layers (0-10m) i.e. a large amount of BSP is accumulated in the North Aegean coastal waters. Moreover, from Figure 16 it is evident that the BSP concentration value increases with respect to time and it stabilizes approximately after 4 years of real flow, which means that at this point the inflow from Dardanelles is equal to the outflow at the open boundary, and therefore a dynamic equilibrium has been reached in the model. Once the model has established a dynamic equilibrium, it is then obvious that it switches to a mode that depends on the transient character of the environmental forcing. The

first four years of the simulation period are more dominated by the transient adjustment response. The concentrations fluctuations with respect to time that are illustrated in Figure 16 show the combination of the model spin-up (transient) response and the response to the time-dependent forcing. As the water depth increases the BSP concentration decreases. It is also evident that the BSP concentration is influenced by the seasonality and the water column stratification. Thus, in late summer – early autumn, when the BSW discharge at the Dardanelles exit is low and a relatively strong stratification is developed in the water column, the BSP concentration is at its maximum value within the first 25 m of depth. In winter, when the BSW discharge at the Dardanelles exit is high and a vertical mixing causes the weakening of the water column stratification, the BSP concentration is at its minimum for depths from 0 to 25 m, and at its maximum for depths from 25 to 50 m. For depths more than 500 m the BSP concentration slightly increases with the time. Thus, at 500m depth the BSP concentration is 12.5%, and at 750m reaches 10.2% of its initial value.

According to Figure 17, the surface BSP concentration shows a maximum at the release point (Dardanelles Exit), decreases rapidly to the south and decreases, at much lower rate, to the north as far as the distance increases. The negative values in the horizontal axis represent the Turkish coastal area that is situated downstream of the BSP release point (Dardanelles exit). More specific, the areas in the North Aegean Coastal Zone that are mostly affected from the BSP discharge are the coastal waters of Alexandroupolis and Maronia, in which the BSP concentration increases up to 80% and 83% respectively of the Dardanelles inflow concentration. The BSP concentration also appears to be high in the coastal waters of Kavala (70%) as well as at the Lagos bay (73%). As it can be seen the distribution of the surface BSP concentration is depicted for four different seasons. In summer and autumn, when a strong stratification is developed in the water column the BSP concentration at the water surface is high, while in winter and spring the BSP concentration is relatively low, especially in the Thracian coastal area.

Figure 18 shows the velocity vectors of the BSW plume and the instantaneous diffusion of the BSP in the North Aegean on April of 2020. As it can be seen the BSP, after its entrance in the North Aegean Sea is separated in three main streams. The first stream is directed rapidly upwards passing between the Island of Imvros (Gokceada) and the Turkish mainland, flowing with a maximum speed of 0.35 m/sec, along the Thracian coastline. The second stream passes through Limnos and Imvros islands, enhancing the anticyclonic movement that is developed in the Samothraki sea basin, while the third stream flows westwards to Limnos Island and heads to the Athos basin.

Figure 19 presents the distribution of the BSP for certain areas situated along the North Aegean coastline, for the year 2020. As previously stated, Maronia, Alexandroupolis and Lagos Bay present higher BSP concentration values than the rest of the areas, from late spring to early autumn. For the Gulfs of Kassandra and Thermaikos the BSP concentration has relatively small seasonal variations, but the concentration of the BSP appears to be considerable high, about 45%.

The use of the conservative tracer in the present paper leads to the determination of critical pollution Zones for the North Aegean coastal waters. The critical Zones are classified according to the accumulation rate of the BSP. Figures 20(a), 20(b), 20(c) and 20(d) present a classification of the North Aegean coastal waters in major cities and places according to their pollution risk due to the predicted BSP concentrations at the end of the numerical simulation (year 2020). According to Figures 20(c) and 20(d), the BSP concentration is in general very high at July and October. The most critical Zones at that period are the coastal waters between Alexandroupolis and Strymonikos Gulf, the north and east part of Thasos Island, the whole coastal region of Samothraki Island and the south and east part of Limnos Island.

5. Conclusions

The present paper describes a combined modeling-observational study of the long-term transport dispersion and accumulation of an assumed passive BSP, represented by the introduction of a conservative passive tracer, in the complex coastal zone of the North Aegean Sea. The BSP is released from the Dardanelles entrance providing thus a monitoring tool for the dispersal of the conservative pollutant in the coastal waters of the North Aegean that originates from the Black Sea. The main conclusions that can be withdrawn from the present paper are summarized below:

(i) The derived surface flow pattern from 3D ELCOM, in the discharge region of the Dardanelles, and the temperature and salinity profiles at Athos area were found to be in satisfactory agreement with the results from Poseidon system of the Hellenic Centre of Marine Research, showing the reliability of the simulation.

(ii) An important volume of the BSP outflow, diverges and accumulates in the North Aegean due to the hydrodynamic circulation that occurs in the area, with major risk, within the next few decades, the environmental degradation of the North Aegean.

(iii) The areas in the North Aegean Coastal waters that are mostly affected by the BSP are the coastal areas from Alexandroupolis to Kavala, situated in the Thracian coastline, the Island of Samothraki, the north and east part of Thassos Island and the south and east part of Limnos Island.

(iv) The BSP concentration in the surface layers of the North Aegean increases with time at faster rates than in the deeper layers. However, for great depths (>500m) the BSP concentration is considerable, showing a slightly increasing trend with respect to time.

(v) The water column stratification that is achieved in late summer-early autumn, increases the surface BSP concentration, while in winter that the vertical mixing causes the weakening of the water column stratification, the BSP concentration is considerably decreased.

Although the North Aegean Sea is still a very clean water basin, there is a high risk of its long-term environmental degradation, due to the BSP accumulation in the coastal areas of the North Aegean, which will dramatically affect its tourism and economic development. The present study successfully evaluates this serious future hazard and estimates the necessity of monitoring this physical event using 3D hydrodynamic models such as ELCOM.

6. Acknowledgement

The authors would like to express their gratitude to all the people who have helped for the production of the present paper. The authors would like to thank especially the CWR (Centre of Water Research) of the University of Western Australia and more specific the director of the CWR Professor Jorg Imberger as well as Dr. Clelia Luisa Marti and Dr. Chris Dallimore for their modeling assistance and support. The authors would also like to acknowledge the generous contribution of data by the Hellenic Centre for Marine Research.

References

Alper, Ö., Almaz, Ílhan Or., Birnur Özbaş., 2006. Investigation of transit Maritime traffic in the Strait of Istanbul through simulation modeling and scenario analysis. International Journal of Simulation – Systems Science & Technology 7, 1-9. Available from: http://www.ijssst.info/.

Androulidakis, Y., Kourafalou, V., 2011. Evolution of a buoyant outflow in the presence of complex topography: The Dardanelles plume (North Aegean Sea), Journal of Geophysical Research 116, 24.

Birpinar, M.E., Talu Gonca, F., Gönül, S., Gülbey, M., 2006. The Effect of Dense Maritime Traffic on the Bosphorus Strait and Marmara Sea Pollution. Conference on Water observation and Information System for Decision Support, BALWOIS 2006, Ohrid, Republic of Macedonia, pp. 1-11.

Blain, C.A., Cambazoglu, M.K., Kourafalou, V.H., 2009. Modeling the Dardanelles Strait outflow plume using a coupled model system. Conference Proceeding of Marine Technology for Our Future: Global and Local Challenges, Biloxi, MS.

Evangeliou, N., Florou, H., Bokoros, P., Scoullos, M., 2009. Temporal and spatial distribution of ^{137}Cs in Eastern Mediterranean Sea. Horizontal and vertical dispersion in two regions. Journal of Environmental Radioactivity 100, 626-636.

Hellenic Centre for Marine Research, Monitoring, Forecasting and Information System for the Greek Seas, 2010, Data Base of Water Temperature and Salinity, HF Remote Sensing – the CORI system, Available from: http://poseidon.hcmr.gr/index.php.

Hodges, B., Dallimore, C., 2010a, ELCOM User Manual, CWR, University of Western Australia.

Hodges, B., Dallimore, C., 2010b. ELCOM Science Manual, CWR, University of Western Australia.

Isari, S., Ramfos, A., Somarakis, S., Koutsikopoulos, C., Kallianiotis, A., Fragopoulu, N., (2006) Mesozooplankton distribution in relation to hydrology of the north-eastern Aegean Sea, eastern mediterranean. Journal of Plankton Research 28, 241–255.

Ignatiades, L., Psarra, S., Zervakis, V., Pagou, K., Souvermezoglou, E., Assimakopoulou, G., Gotsis-Skretas, O., 2002.Phytoplankton size-based dynamics in the Aegean Sea (Eastern Mediterranean). Journal of Marine Systems 36, 11-28.

Ignatiades, L., 2005. Scaling the trophic status of the Aegean Sea, eastern Mediterranean. Journal of Sea Research 54, 51-57.

Imberger, J., J.Patterson., 1990. Physical limnology. Advances in Applied Mechanics 27, 303-475.

Kanarska, Y., Maderich, V., 2008.Modelling of seasonal exchange flows through the Dardanelles Strait. Estuarine, Coastal and Shelf Science 79, 449–458.

Kontoyiannis, H., Kourafalou, V.H., Papadopoulos, V., 2003. The seasonal characteristics of the hydrology and circulation in the northwest Aegean Sea (eastern Mediterranean): Observations and Modeling. Jourrnal of Geophysical Research, 108, 18.1-18.23.

Korres, G., Lascaratos, A., Hatziapostolou, E. and Katsafados, P., 2002. Towards an ocean forecasting system for the Aegean Sea. Journal of Atmospheric & Ocean Science 8, 191-218.

Koukouras, A., Voultsiadou-Koukouras, E., Kattoulas, M., 1984. Benthic bionomy of the North Aegean Sea. I. Physico-chemical characteristics of the Strymonikos Gulf. Thalassia Jugoslavica 20, 53-72.

Kourafalou, V.H., Barbopoulos, K., 2003. High resolution simulations on the North Aegean Sea seasonal circulation. Annales Geophysicae 21, 251-265.

Ludwig, W., Dumont, E., Meybeck, M., Heussner, S., 2009. River discharges of water and nutrients to the Mediterranean and Black Sea: Major drivers for ecosystem changes during past and future decades? Progress in Oceanography, 80, 199-217.

Olson, D.B., Kourafalou, V.H., Johns, W.E., Samuels, G. and Veneziani, M., 2006. Aegean Surface Circulation from a Satellite - Tracked Drifter Array. Journal of Physical Oceanography 37, 1898-1917.

Sylaios, G., Koutrakis, E., Kallianiotis, A., 2006. Hydrographic variability, nutrient distribution and water mass dynamics in Strymonikos Gulf (Northern Greece). Continental Shelf Research 26, 217-235.

Tzali, M., Sofianos, S., Mantziafou, A., Skliris, N., 2010. Modelling the impact of Black Sea water inflow on the North Aegean Sea hydrodynamics. Ocean Dynamics 60, 585-596.

Unluata, U., Oguz, T., Latif, M.A. and Ozsou, E., 1990. On the physical oceanography of the Turkish Straits. In: L.J. Pratt (Eds), The Physical Oceanography of Sea Straits, Kluwer Academic Publishers, pp. 25-60.

Zaitsev, Y. and Mamaev, V., 1997. Marine Biology Diversity in the Black Sea – A Study of Change and Decline, Black Sea Environmental Series, Volume 3.

Figure Captions

Figure 1 Top view of North Aegean Sea bathymetry and computational grid that have been constructed for the simulation in the present work.

Figure 2 Open southern boundary forcing conditions for ELCOM, (a)Salinity, (b)Water temperature (Hellenic Centre for Marine Research, 2010).

Figure 3 Time series of meteorological data recorded at the Genisea station in 2010.

Figure 4 Diagram of the wind velocity and wind direction, recorded at the Genisea station in 2010.

Figure 5 (a),(b),(c),(d) Comparison of modeled (ELCOM) and measured (Poseidon) average water temperature, and (e),(f),(g),(h) comparison of modeled (ELCOM) and measured (Poseidon) average water salinity at Athos Station in 2009 for a range of water depths.

Figure 6 Comparison of modeled and measured data at Athos station for (a) temperature and (b) salinity, for the years 2009 and 2010.

Figure 7 (a),(b),(c) Comparison of modeled (ELCOM) and measured (Evangeliou et al., 2009) water temperature, and (d),(e),(f) comparison of modeled (ELCOM) and measured (Evangeliou et al., 2009) water salinity at Stations L.1, L.2 and L.3 on December 2005 for a range of water depths.

Figure 8 Comparison of modeled (ELCOM) and measured (Evangeliou et al., 2009) density profiles at Stations L.1, L.2 and L.3 on June 2006.

Figure 9 Comparison of modeled and measured data at stations L.1, L.2 and L.3 for (a) temperature and (b) salinity, for December 2009. (c) Comparison of modeled and observed density data, for June 2010.

Figure 10 (a),(b)Modeled velocities of the surface currents in the region close to the Dardanelles Straits and (c),(d) SC images from CORI surface currents measuring system (Hellenic Centre for Marine Research, 2010), for 8 February 2010 and 25 September 2010 respectively.

Figure 11 Average monthly surface salinity values distribution in the North Aegean Mainland coastal waters in the year 2010. The horizontal axis concerns the distance in km along the coastline in a counter-clockwise direction, with the zero value located at the Dardanelles exit. The negative values in the horizontal axis represent the Turkish coastal area that is situated downstream of the BSP release point (Dardanelles exit).

Figure 12 Average monthly surface temperature values distribution in the North Aegean Mainland coastal waters in the year 2010. The horizontal axis concerns the distance in km along the coastline with a counter-clockwise direction, with the zero value located at the Dardanelles exit. The negative values in the horizontal axis represent the Turkish coastal area that is situated downstream of the BSP release point (Dardanelles exit).

Figure 13 Surface density and current velocity in the North Aegean during the spring and summer period of the year 2009.

Figure 14 Modeled surface water circulation, in a typical summer day of the year 2008, in the North Aegean Sea.

Figure 15 Instantaneous distribution of the surface salinity and velocity vectors in the North Aegean water surface on 16th of September of 2010. The image shows the hydrodynamic effect of the BSW plume in the area of Thermaikos Gulf.

Figure 16 Average values of the BSP concentration in the entire domain of the North Aegean, for various depths.

Figure 17 Seasonal Surface distribution of the BSP in the North Aegean Coast in the year 2020, as a function of the distance in km along the coastline. The horizontal axis concerns the distance in km along the coastline with a counter-clockwise direction, with the zero value located at the Dardanelles exit. The negative values in the horizontal axis represent the Turkish coastal area that is situated downstream of the BSP release point (Dardanelles exit).

Figure 18 Instantaneous distribution (26 April 2020) of the BSP concentration and the velocity vectors in the North Aegean surface. It is evident that the BSW plume heads to the North Aegean mainland coastline by three different directions.

Figure 19 Annual variation of BSP concentration series for a variety of coastal areas in the North Aegean.

Figure 20 BSP concentration Zones in the North Aegean coast in (a) winter (b) spring, (c) summer and (e) autumn of 2020.

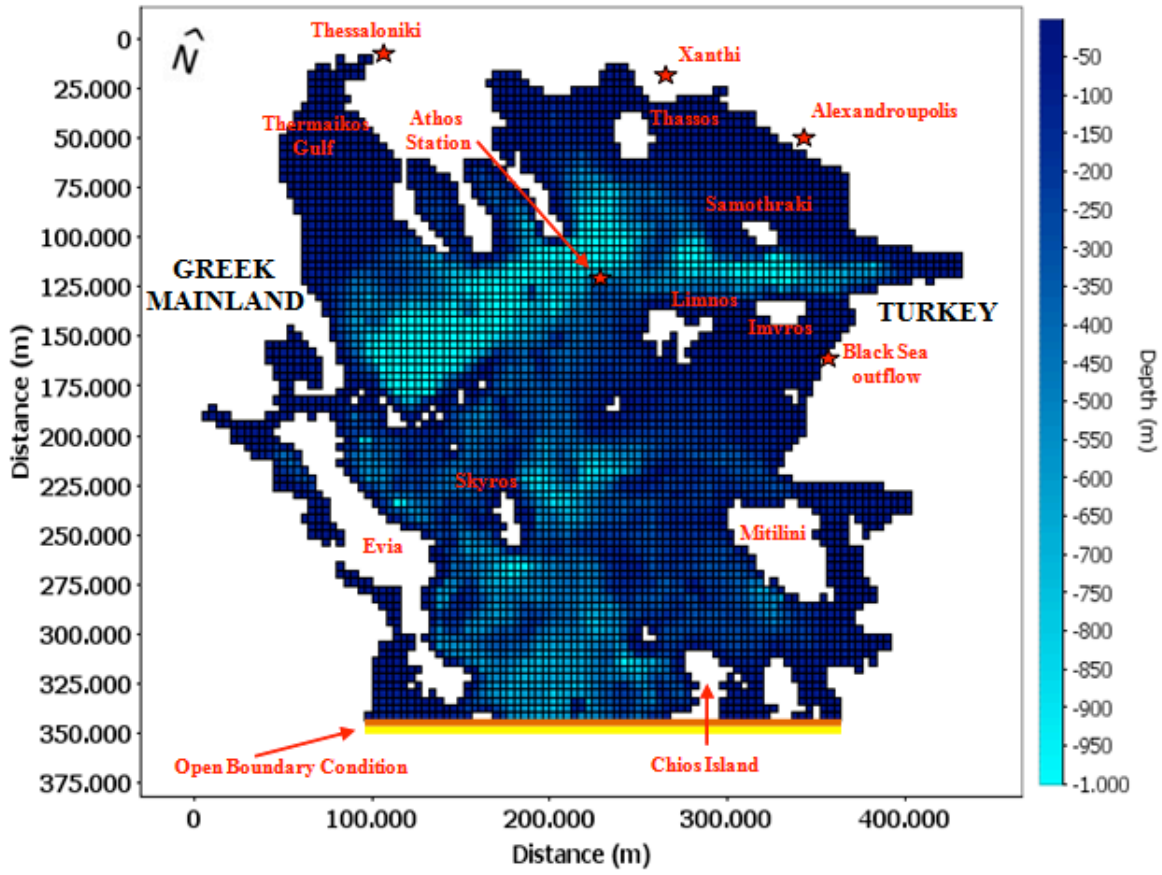

Figure 1.

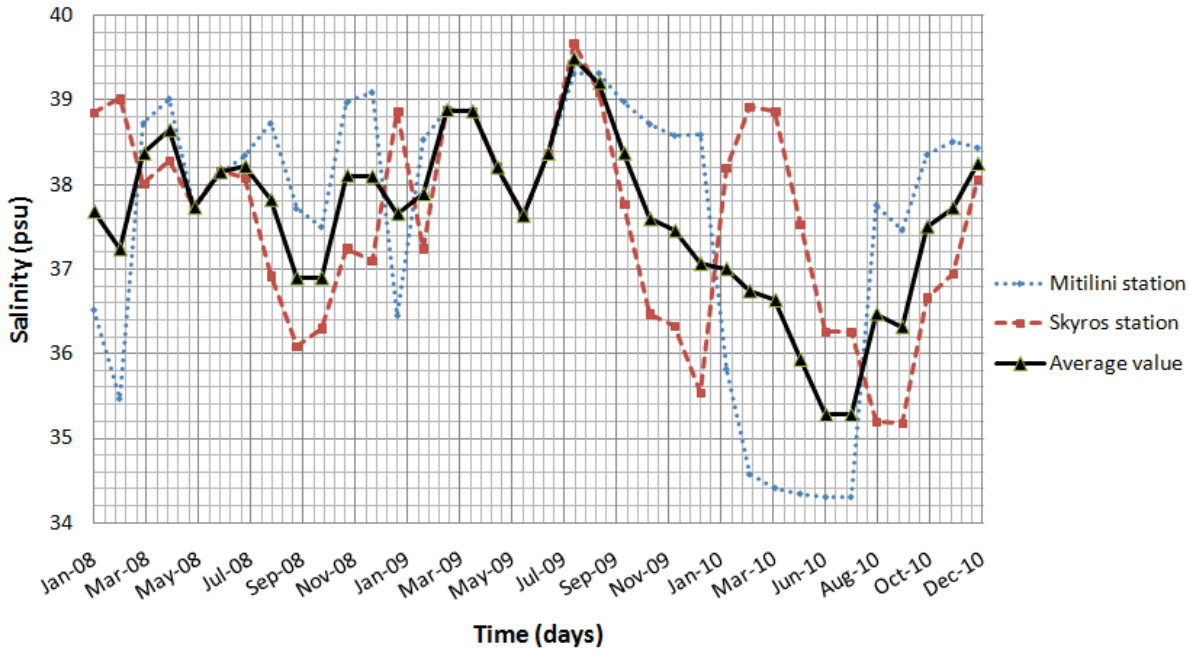

Figure 2(a)

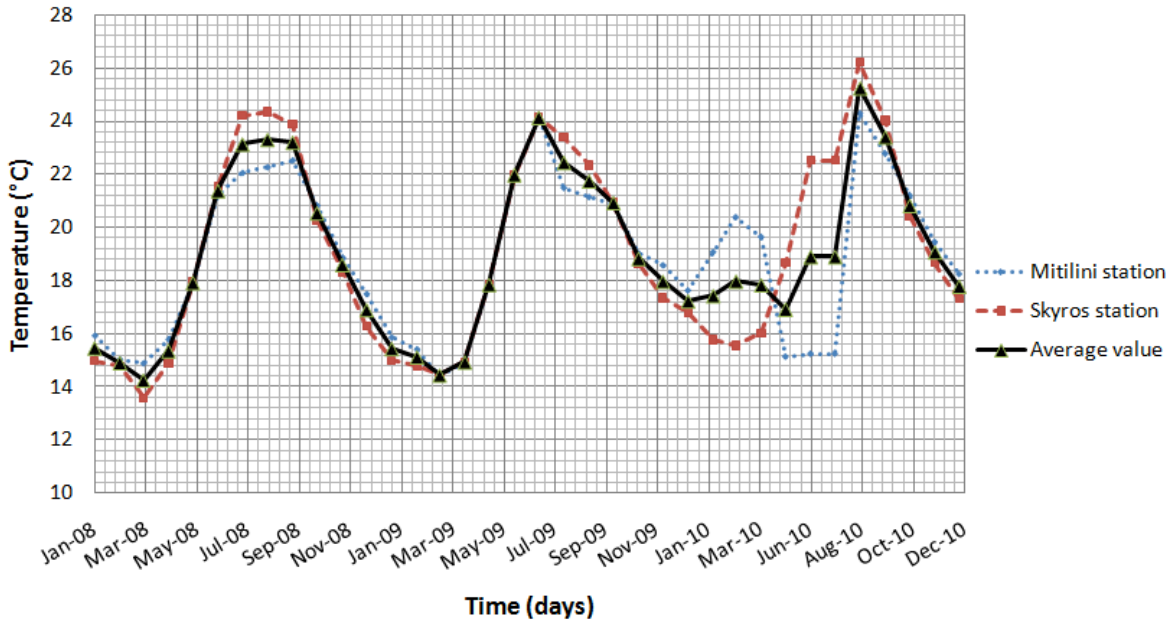

Figure 2(b)

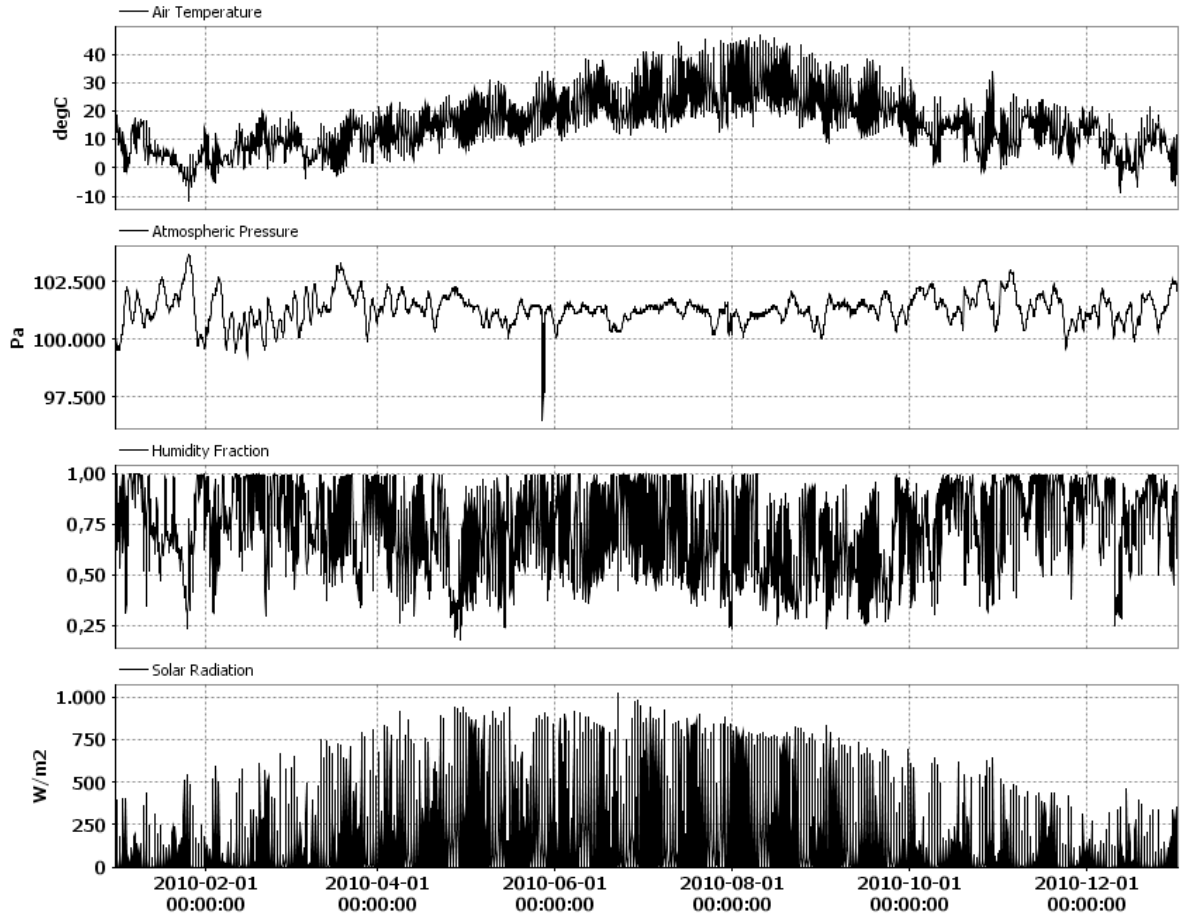

Figure 3.

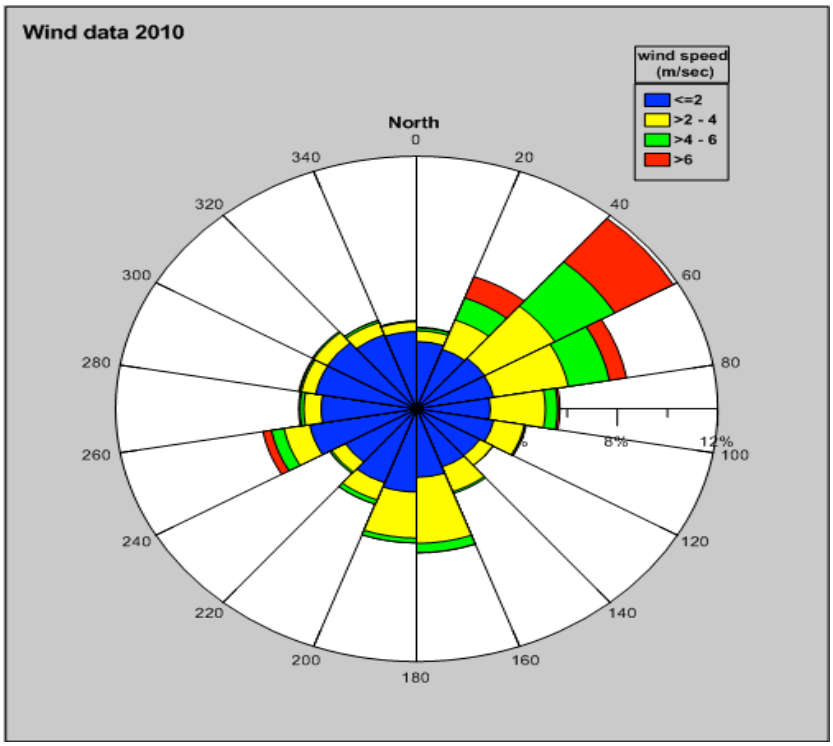

Figure 4.

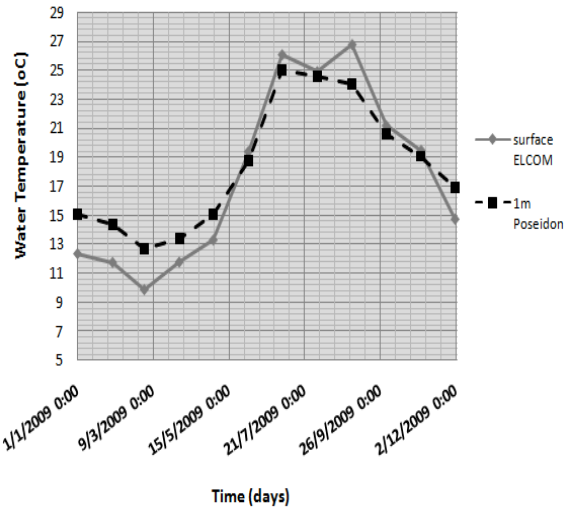

Figure 5(a)

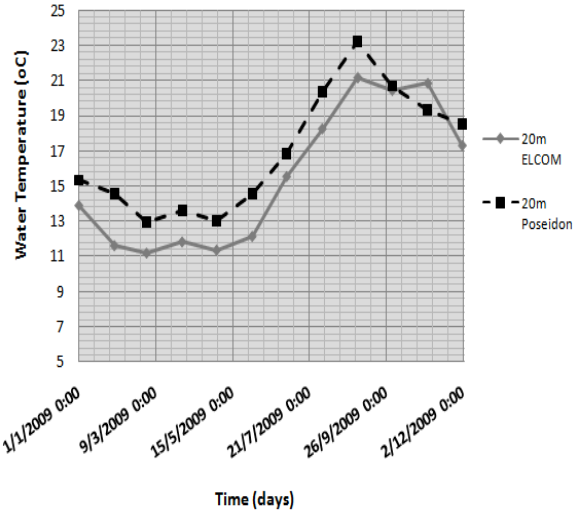

Figure 5(b)

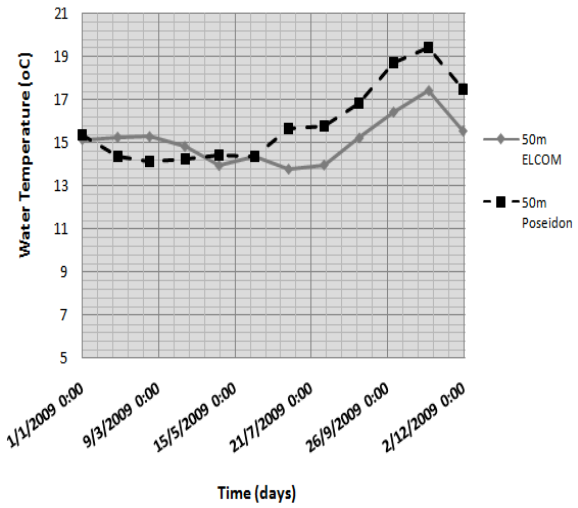

Figure 5(c)

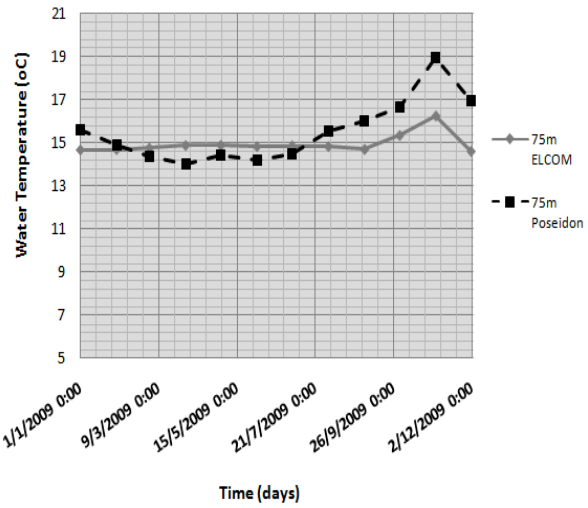

Figure 5(d)

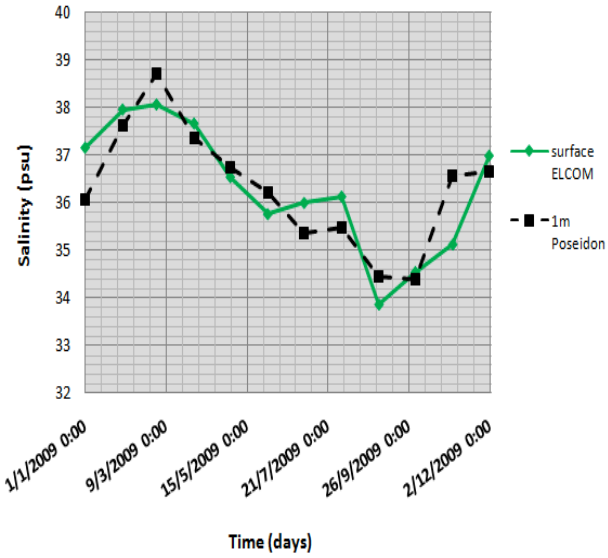

Figure 5(e)

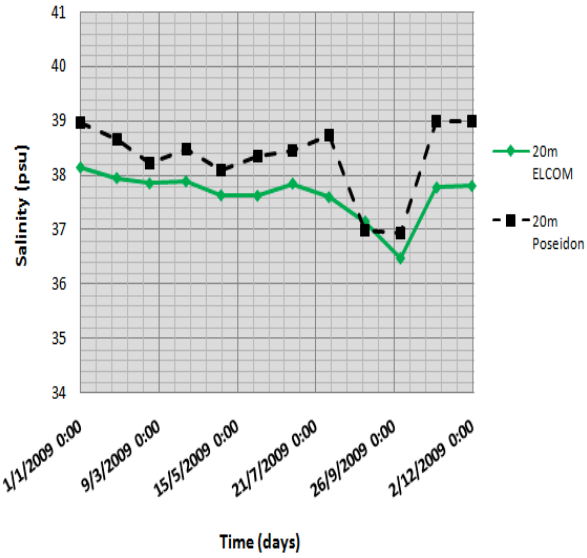

Figure 5(f)

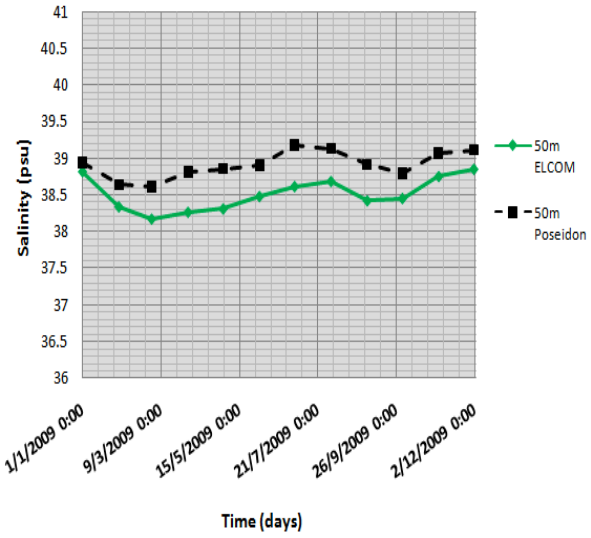

Figure 5(g)

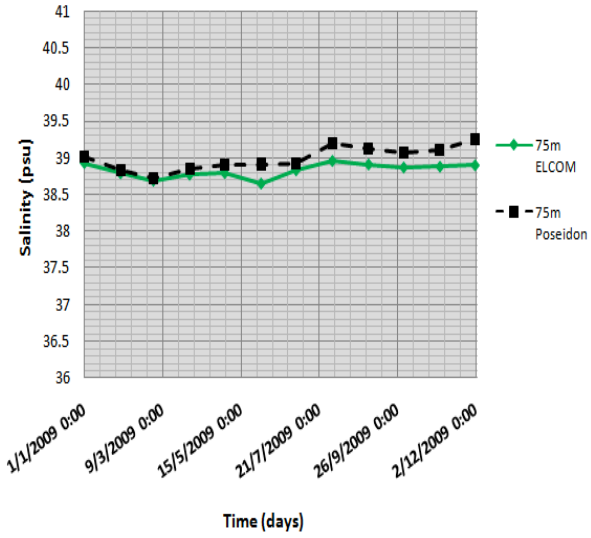

Figure 5(h)

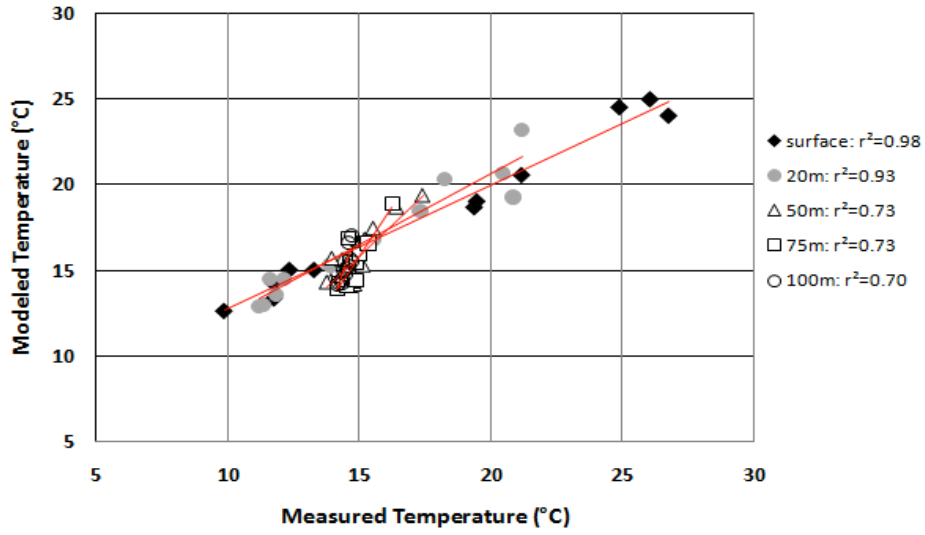

Figure 6(a)

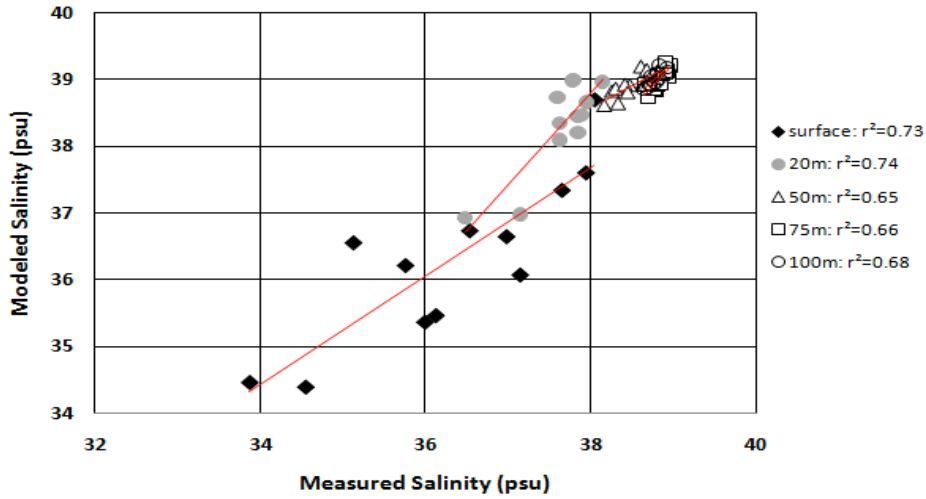

Figure 6(b)

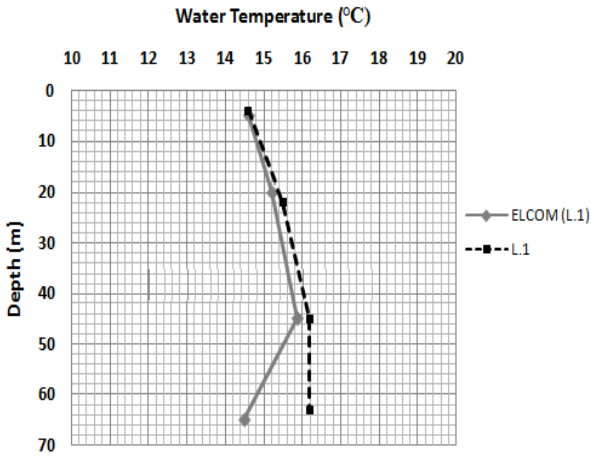

Figure 7(a)

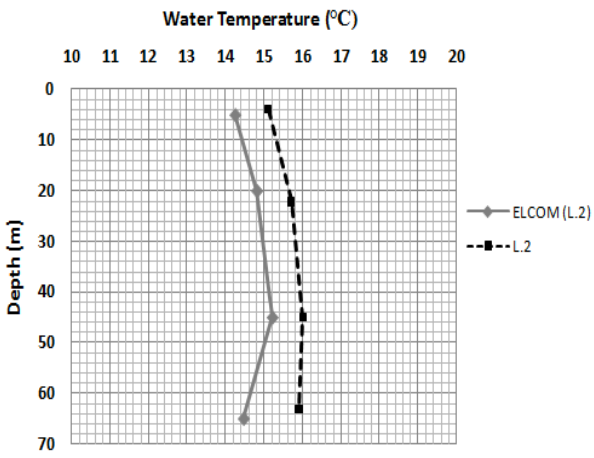

Figure 7(b)

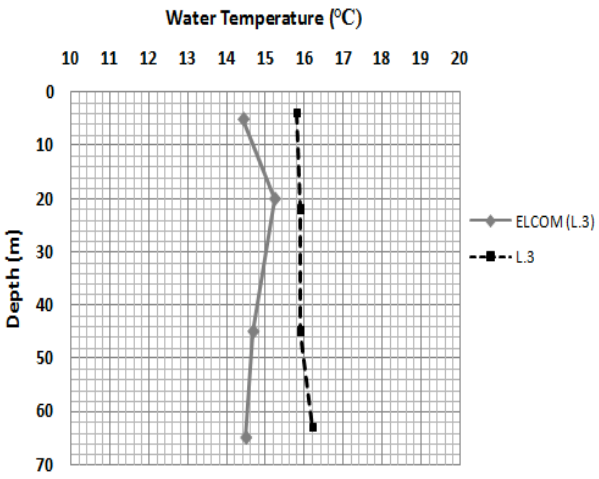

Figure 7(c)

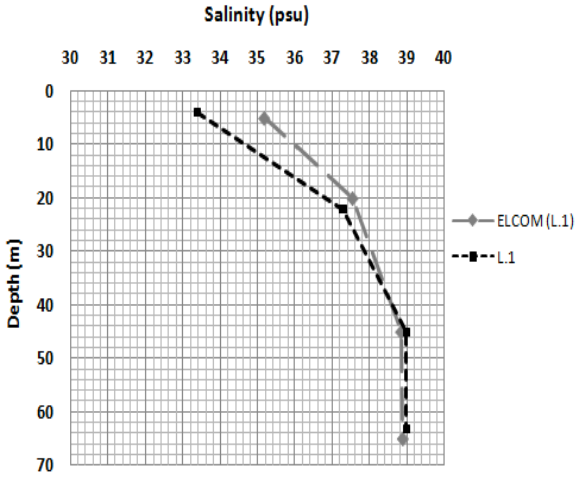

Figure 7(d)

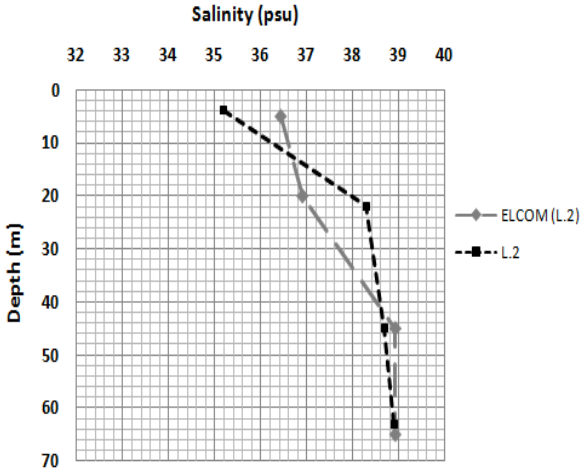

Figure 7(e)

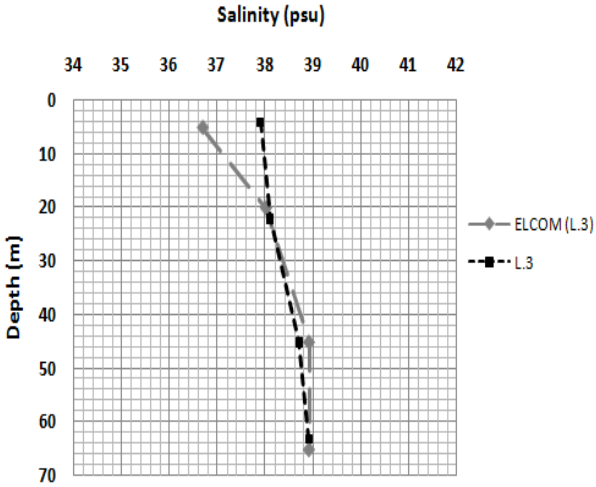

Figure 7(f)

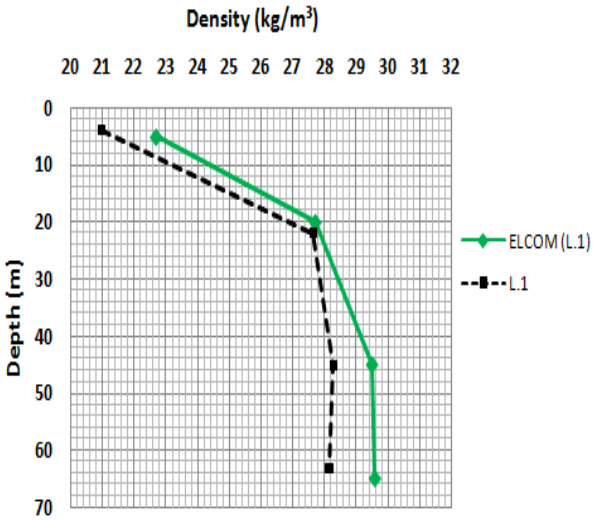

Figure 8(a)

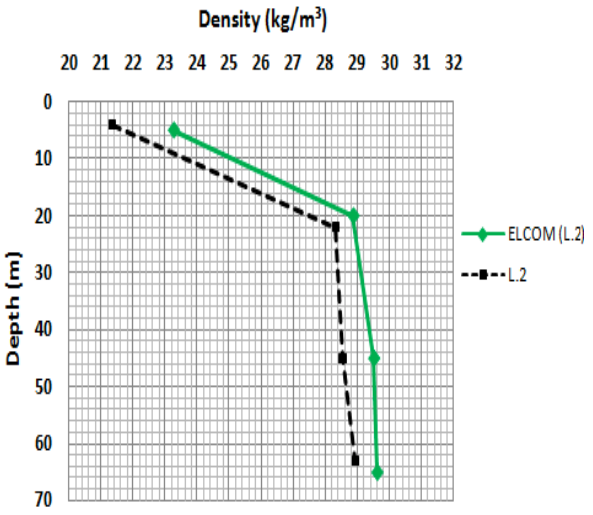

Figure 8(b)

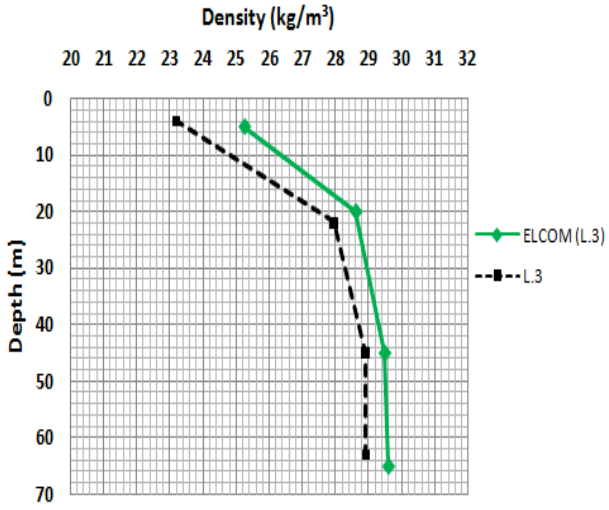

Figure 8(c)

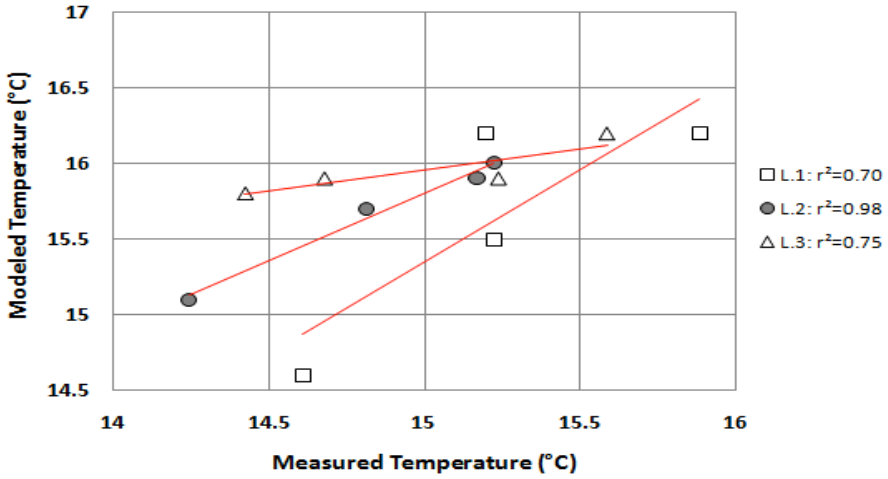

Figure 9(a)

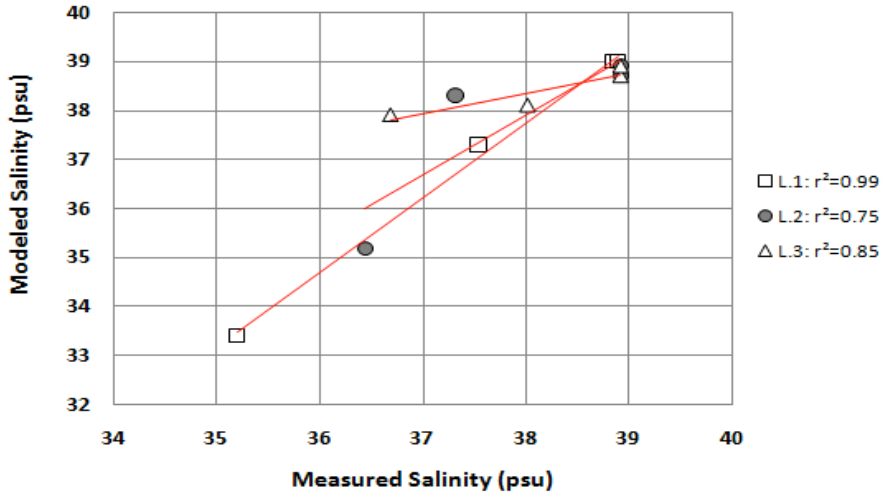

Figure 9(b)

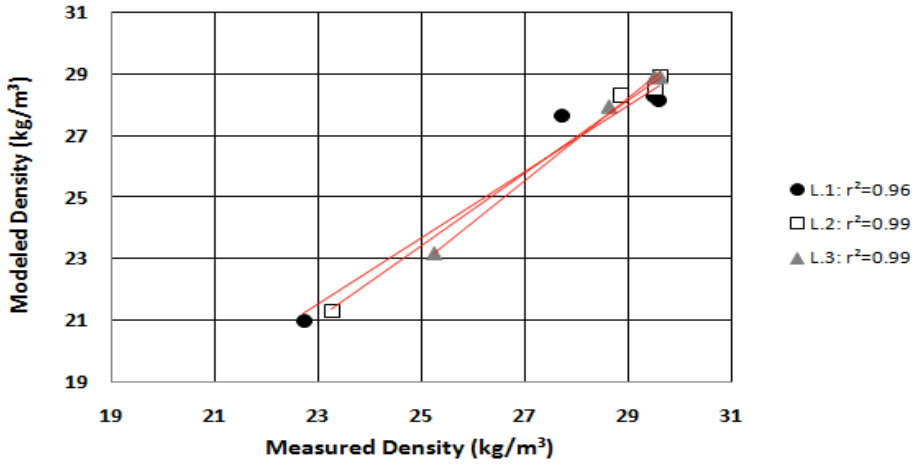

Figure 9(c)

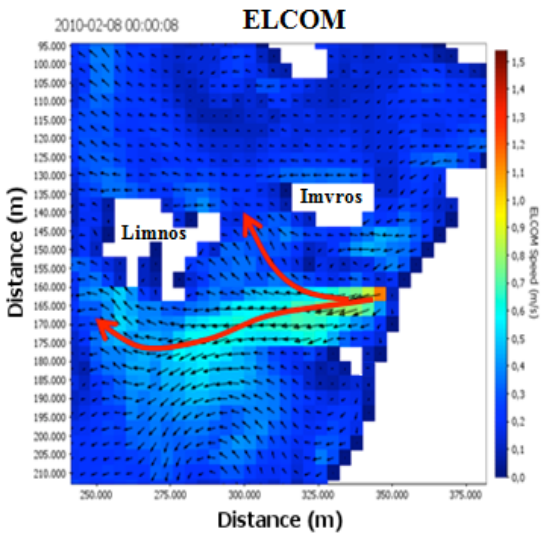

Figure 10(a)

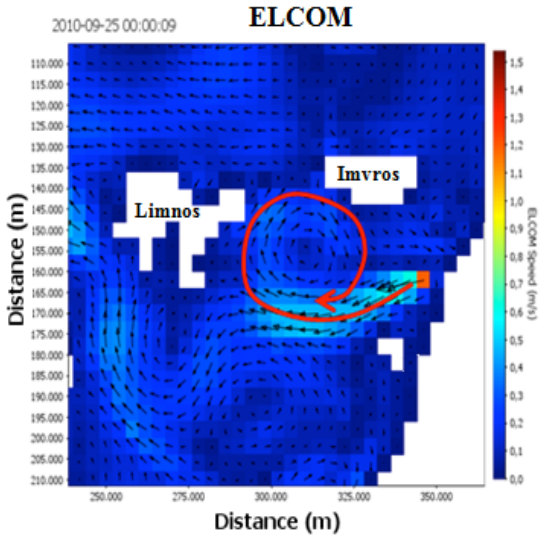

Figure 10(b)

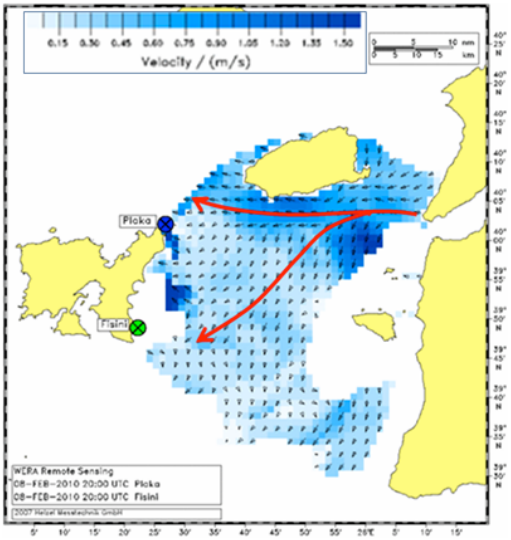

Figure 10(c)

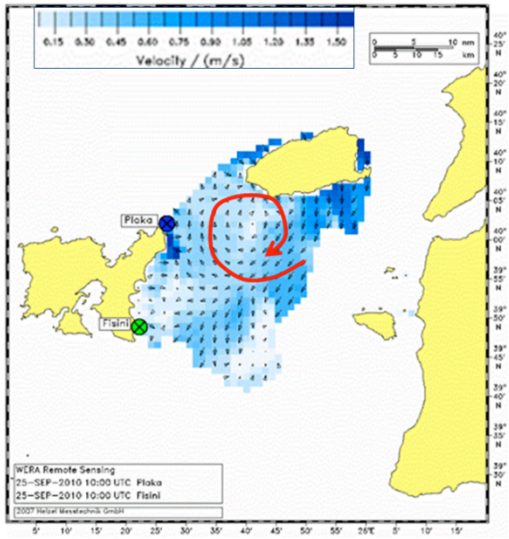

Figure 10(d)

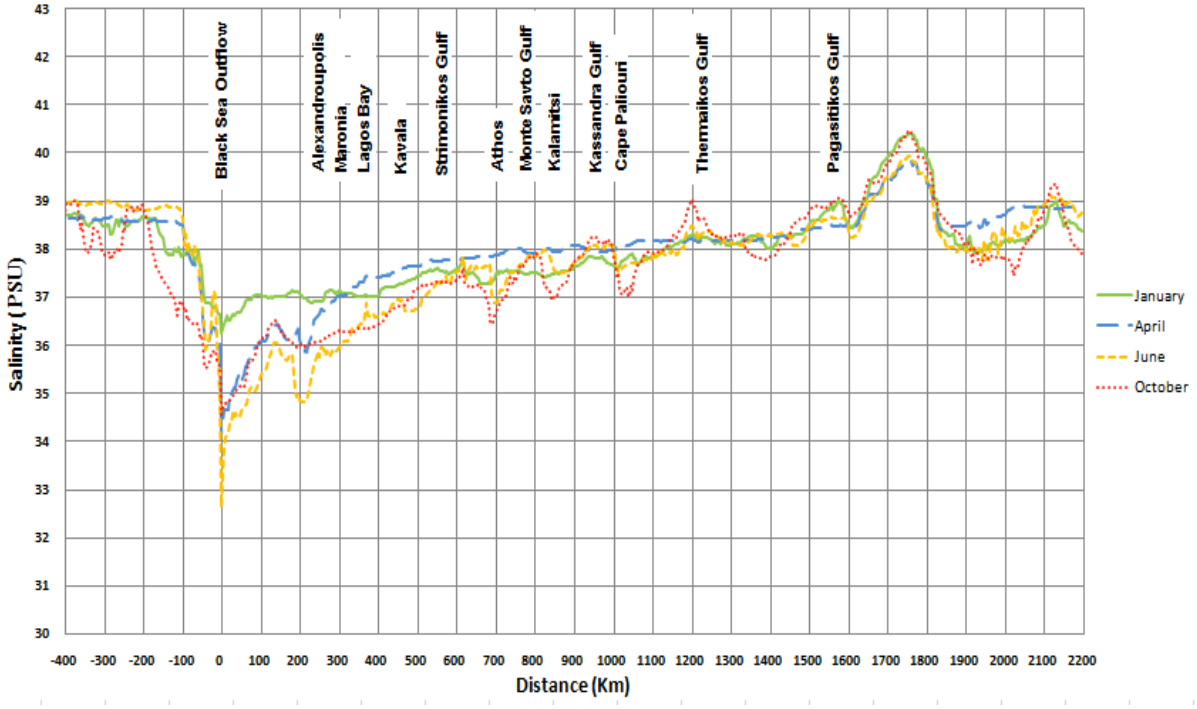

Figure 11.

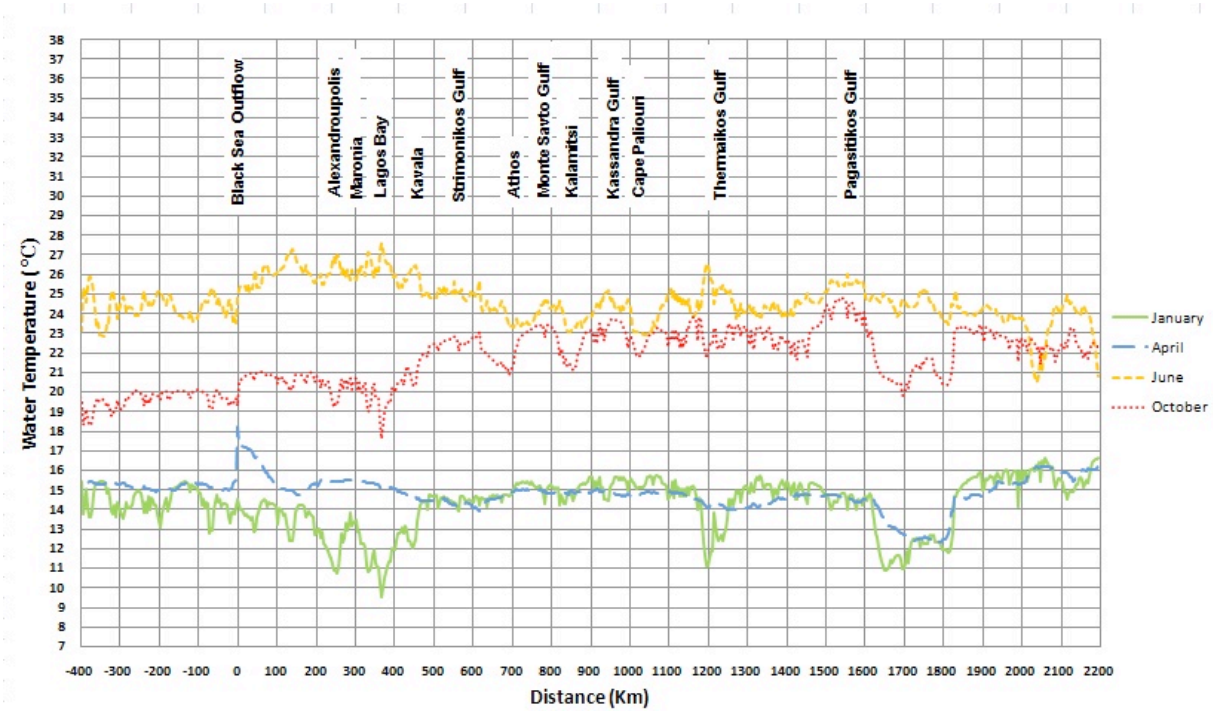

Figure 12.

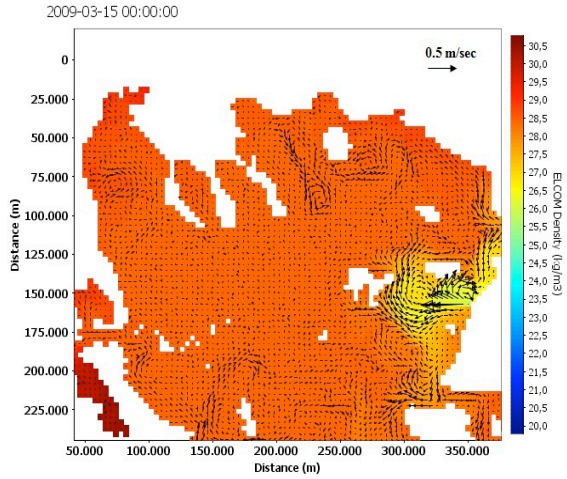

Figure 13(a)

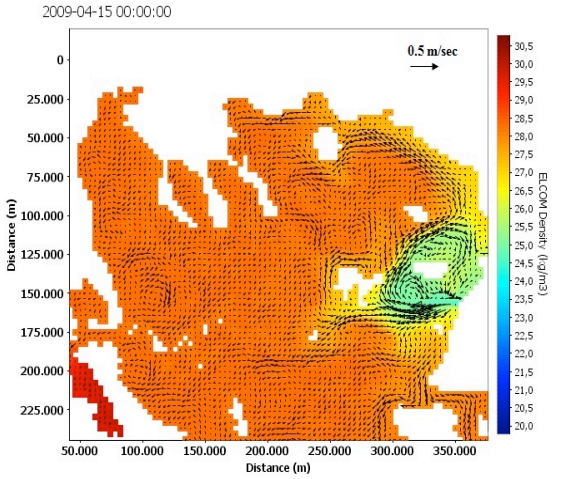

Figure 13(b)

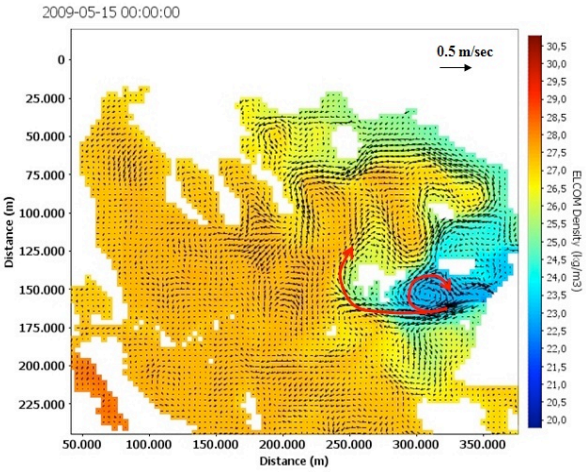

Figure 13(c)

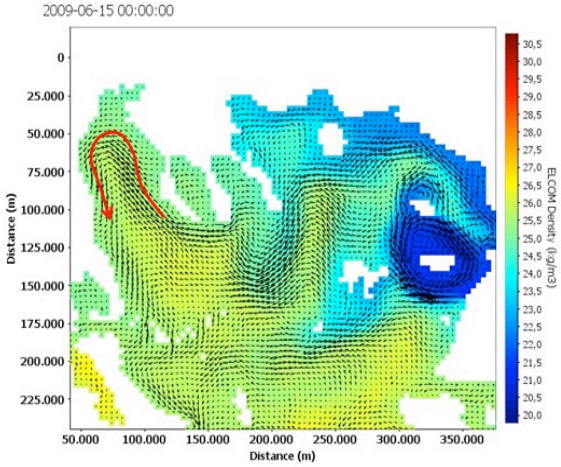

Figure 13(d)

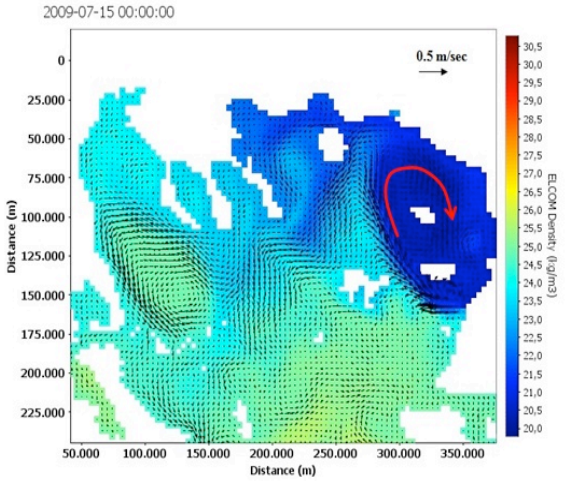

Figure 13(e)

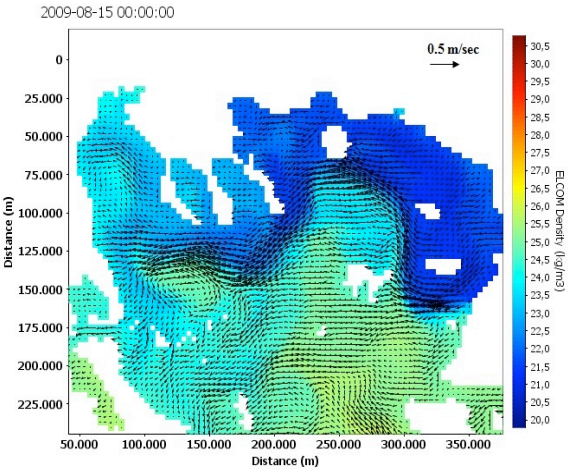

Figure 13(f)

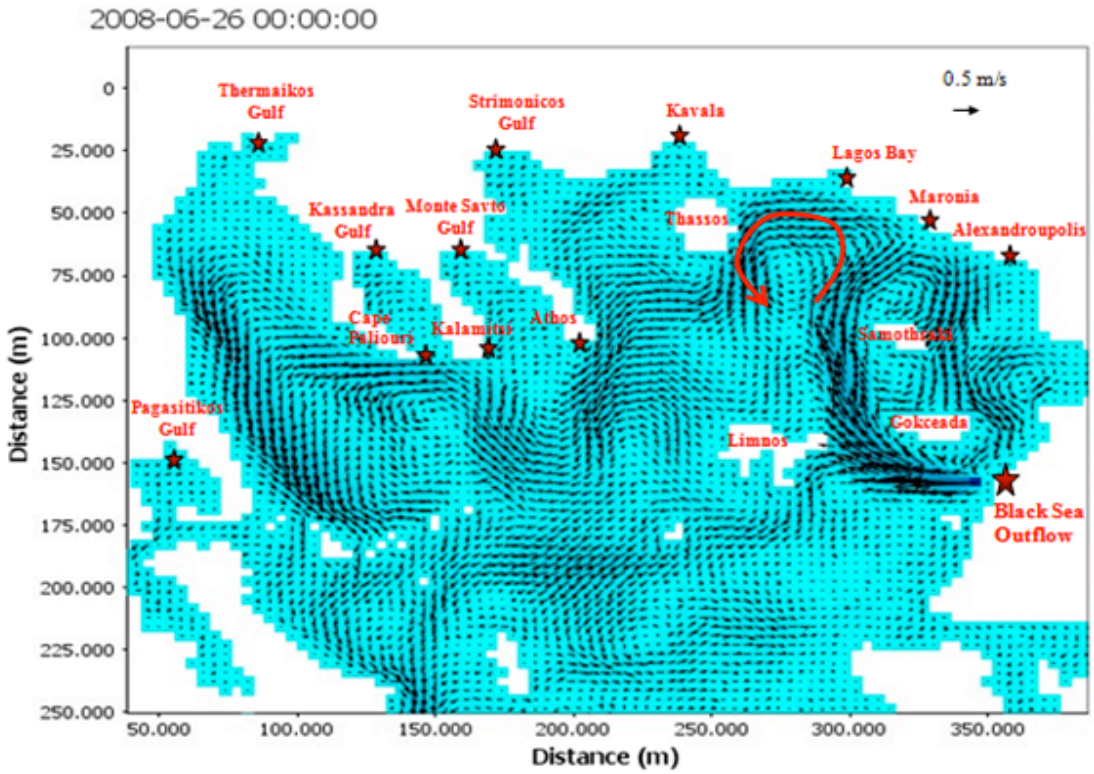

1

2 Figure 14.

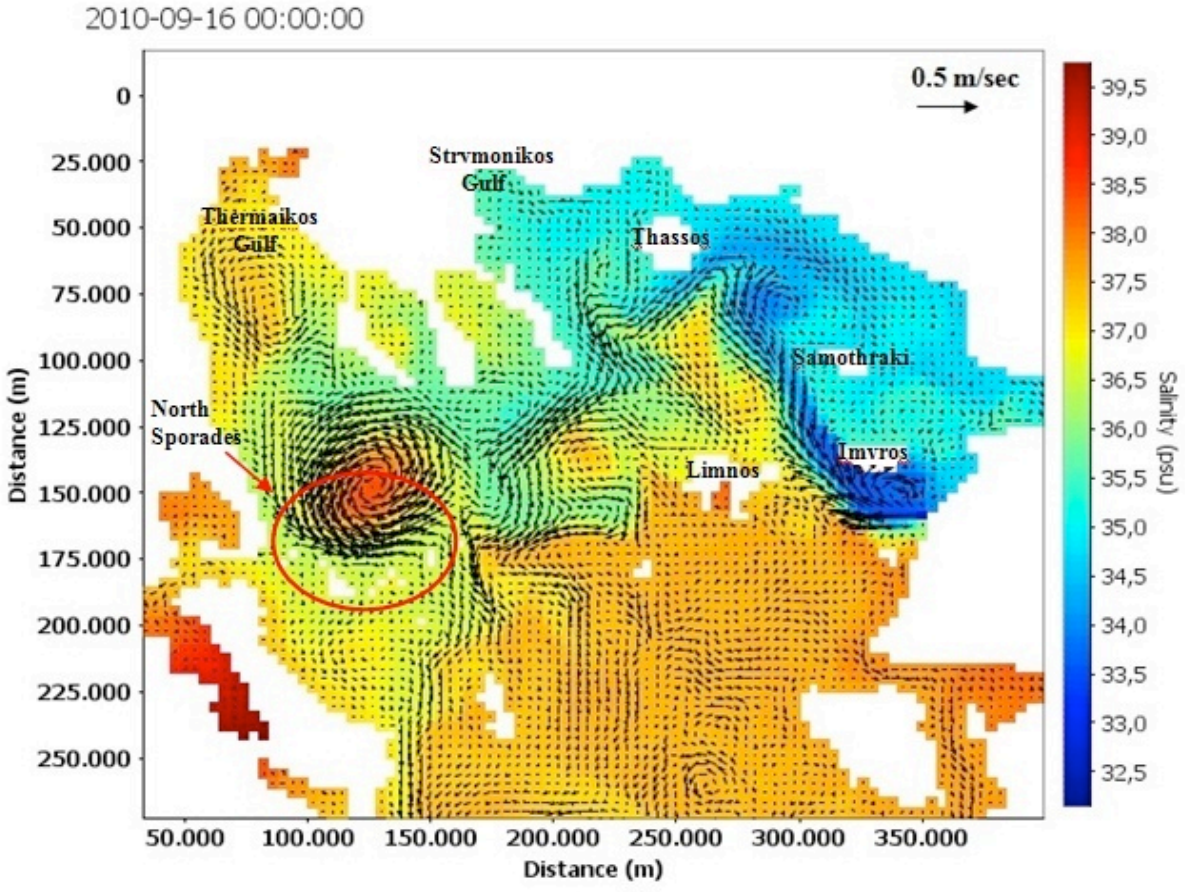

3

4 Figure 15.

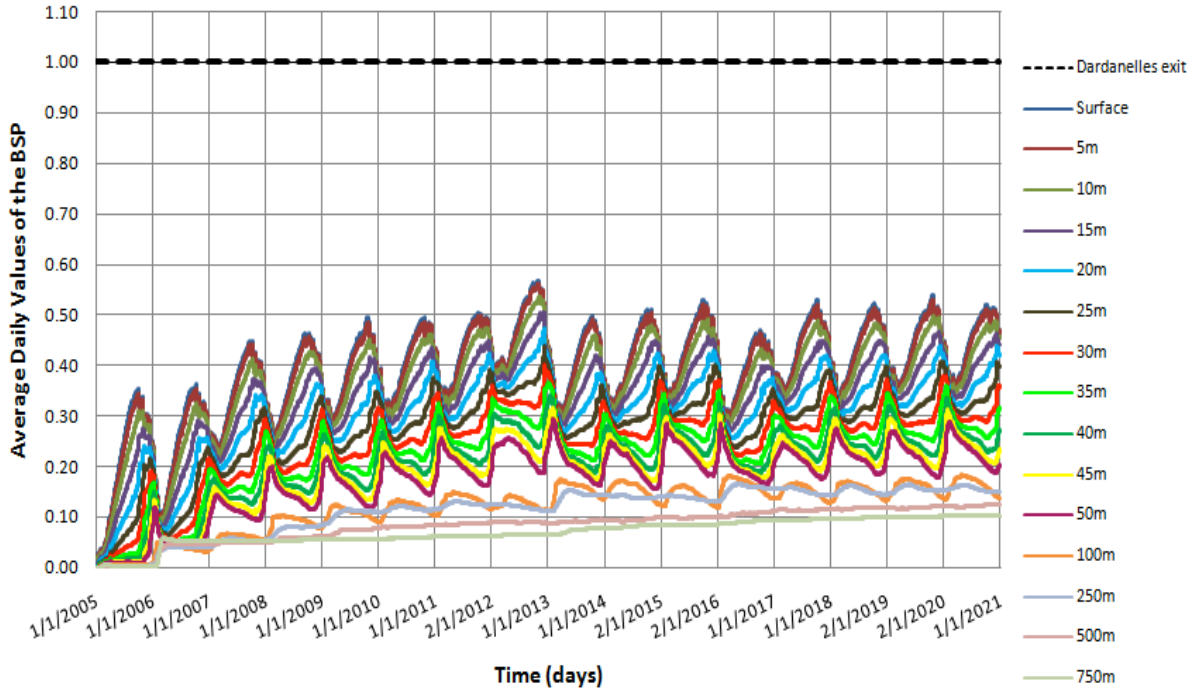

Figure 16.

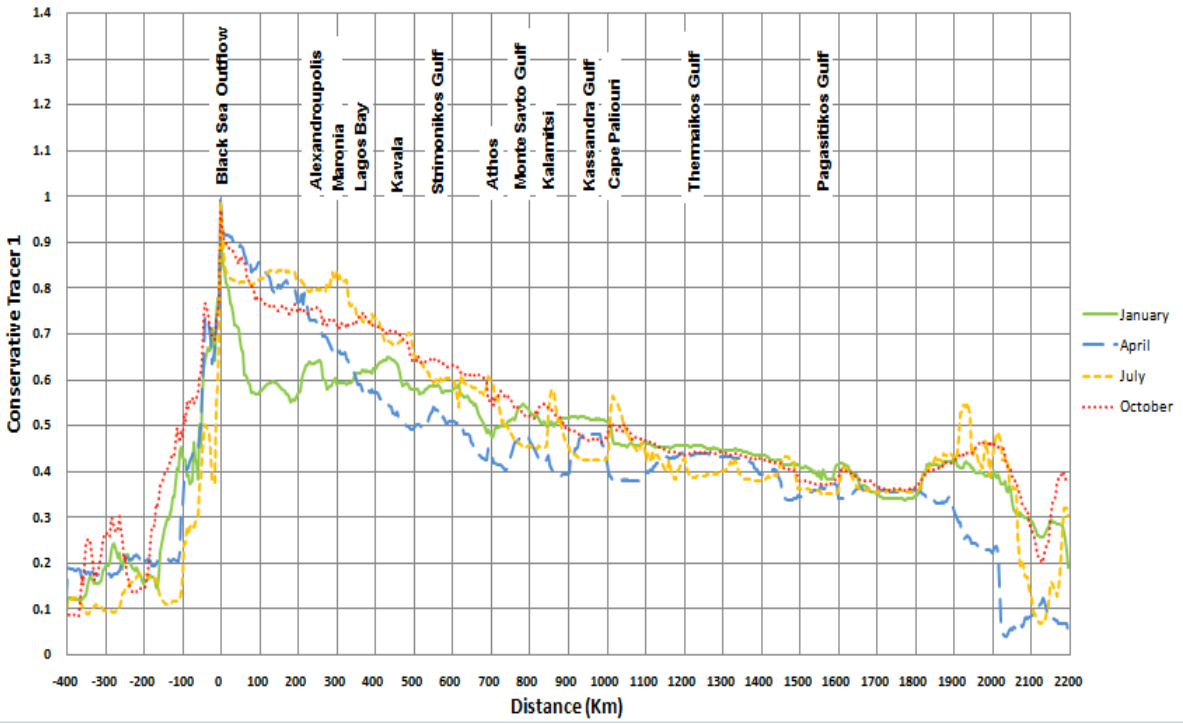

Figure 17.

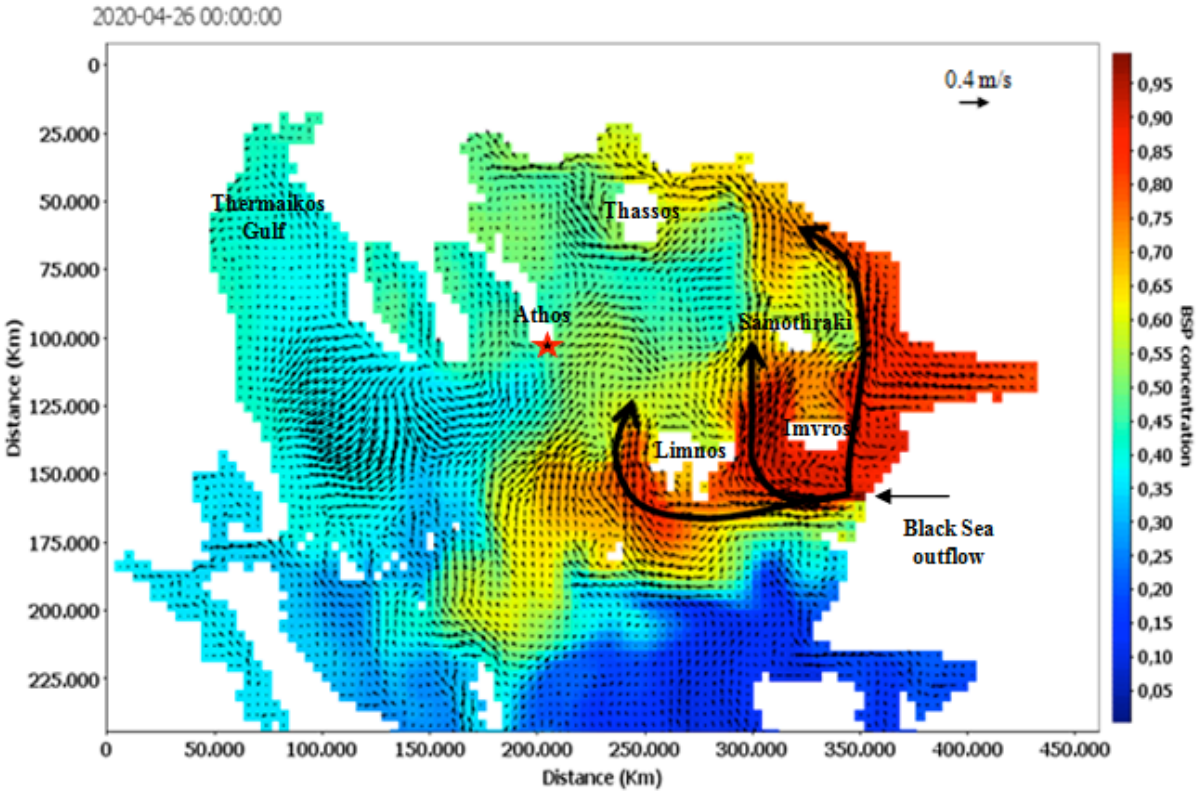

Figure 18.

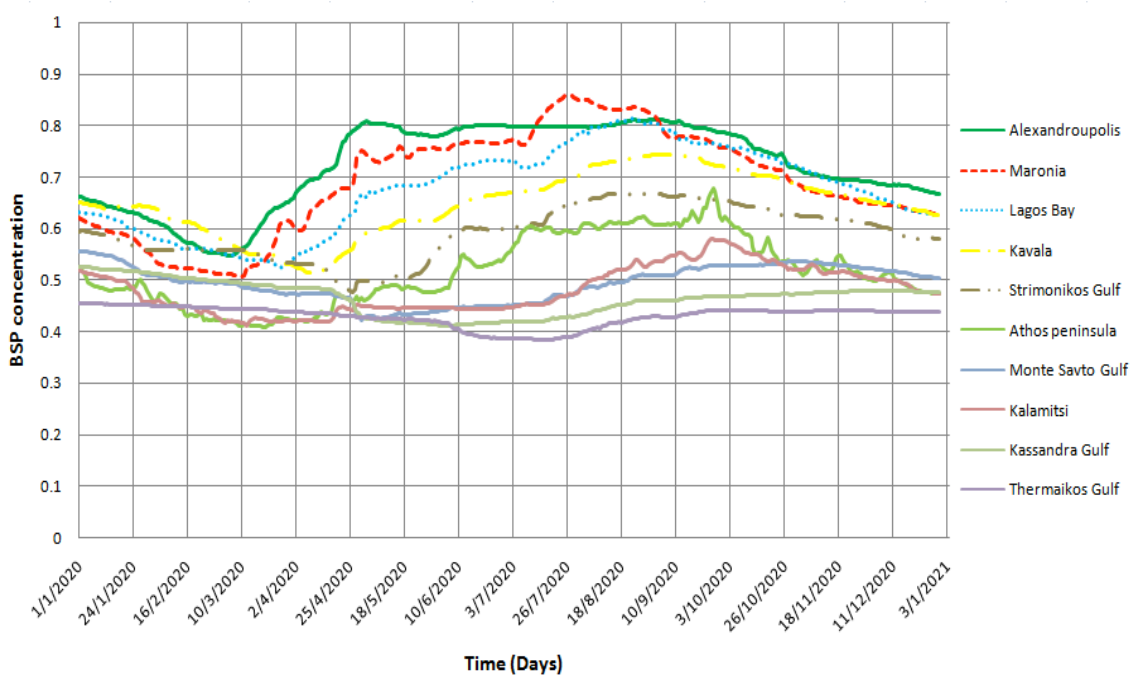

Figure 19.

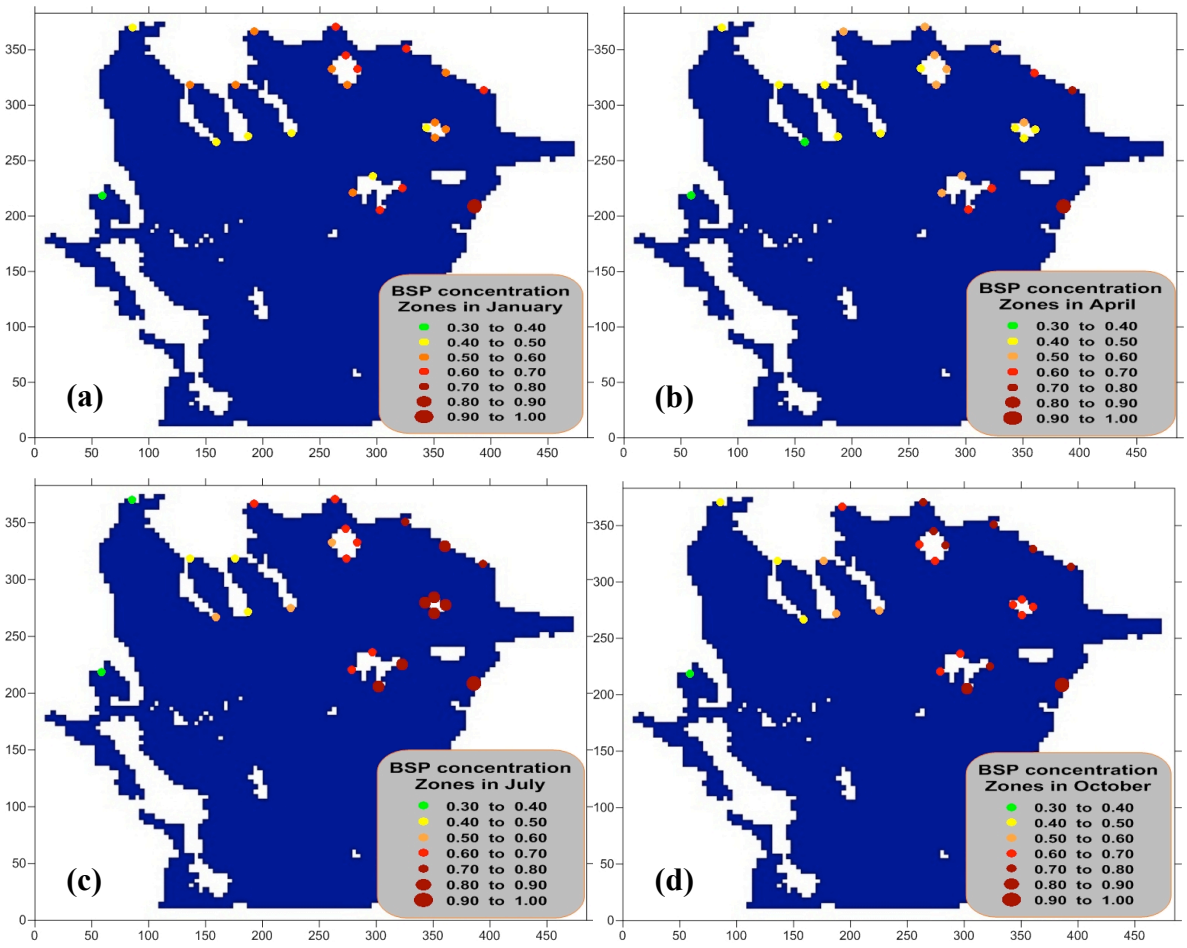
(a)
BSP concentration
Zones in January
0.30 to 0.40
0.40 to 0.50
0.50 to 0.60
0.60 to 0.70
0.70 to 0.80
0.80 to 0.90
0.90 to 1.00
(b)
BSP concentration
Zones in April
0.30 to 0.40
0.40 to 0.50
0.50 to 0.60
0.60 to 0.70
0.70 to 0.80
0.80 to 0.90
0.90 to 1.00
(c)
BSP concentration
Zones in July
0.30 to 0.40
0.40 to 0.50
0.50 to 0.60
0.60 to 0.70
0.70 to 0.80
0.80 to 0.90
0.90 to 1.00
(d)
BSP concentration
Zones in October
0.30 to 0.40
0.40 to 0.50
0.50 to 0.60
0.60 to 0.70
0.70 to 0.80
0.80 to 0.90
0.90 to 1.00

Figure 20